AD-A115 627 AIR FORCE INST OF TECH WRIGHT-PATTERSON AFB OH SCHOO--ETC F/G 17/8
REMOTE SENSING OF GASES USING LIDAR RESONANCE SCATTERING TECHNI--ETC(U)
DEC 81 G C KWEDER
UNCLASSIFIED AFIT/GEP/PH/81D-5 NL

END
DATE FILMED
07-82
DTIC

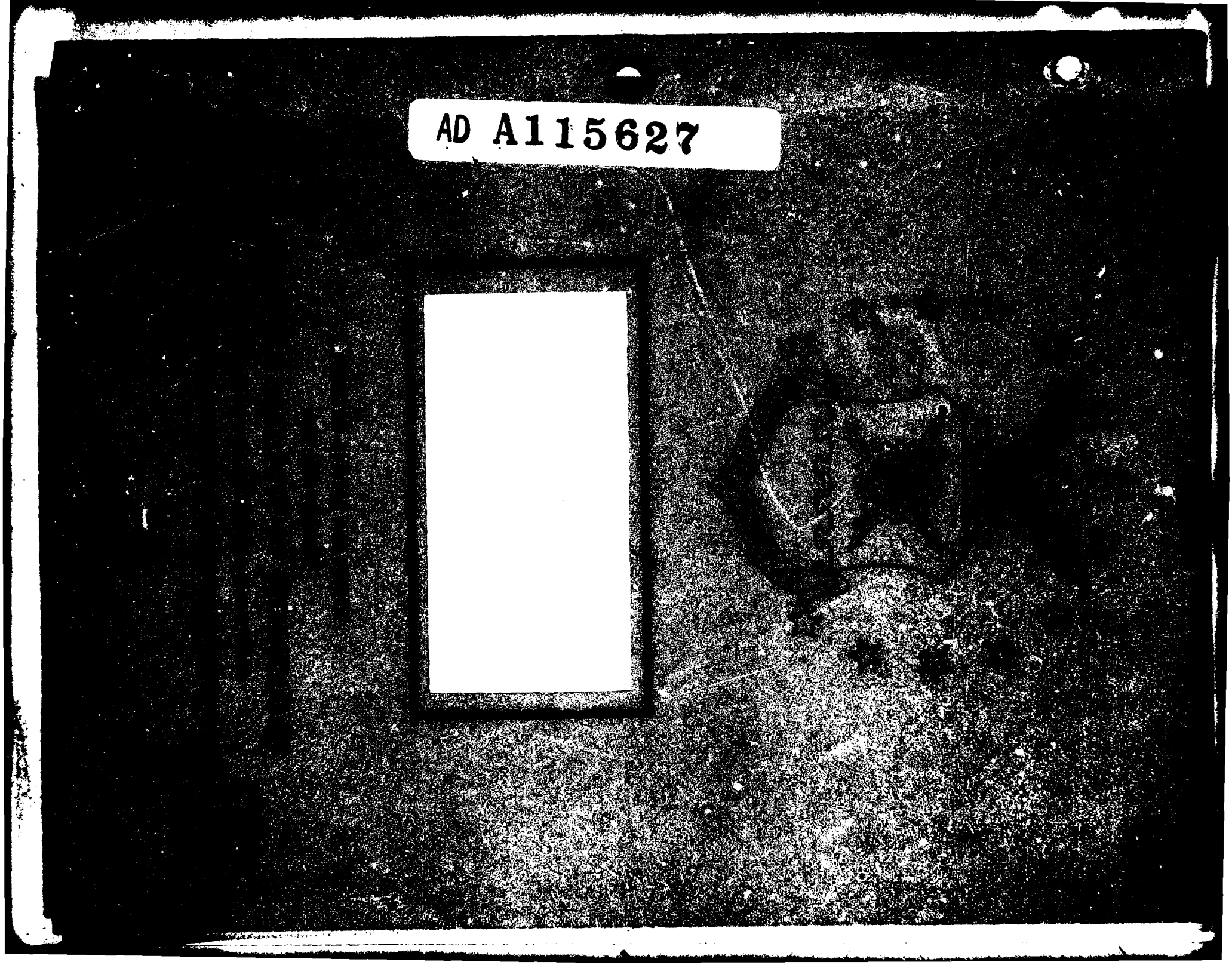

AFIT/GEP/PH/81D-5

REMOTE SENSING OF GASES USING LIDAR RESONANCE SCATTERING TECHNIQUES FROM THE SPACE SHUTTLE

THESIS

Glenn C. Kweder
AFIT/GEP/PH/81D-5 Capt USAF

AFIT/GEP/PH/81D-9 5

REMOTE SENSING OF GASES USING LIDAR RESONANCE SCATTERING TECHNIQUES FROM THE SPACE SHUTTLE

THESIS

Presented to the Faculty of the School of Engineering

of the Air Force Institute of Technology

Air University

In Partial Fulfillment of the

Requirements for the Degree of

Master of Science

by

Glenn C. Kweder

Capt USAF

Graduate Engineering Physics

October 1981

Approved for public release; distribution unlimited

Preface

This thesis is concerned with investigating the feasibility of remote sensing of various types of atoms and molecules by using laser induced resonance-fluorescence techniques from an orbiting platform. A laser, if tuned to the correct frequency, will excite a resonance line of an atom or molecule. If the particle reradiates, it does so at a frequency that is characteristic of that particle. Detection of this signature allows verification of the presence of the particular species. I hope that this work will be useful in evaluating the feasibility of laser remote sensing from space and hopefully my master's degree will bring me one step closer to obtaining my ultimate goal of flying in space and perhaps performing this very experiment.

I would like to thank my advisor, MAJ Lange for sharing his extensive knowledge of this field with me and for being so patient and pleasant during our work together. I would also like to thank my wife, Mary Ann, and my children, Wendy and Eric for putting up with all of the problems that a typical tour of AFIT presents. Finally, I would like to thank God for the inner strength necessary to keep going and never giving up during these past eighteen months.

Glenn Kweder

Abstract

Remote sensing from the space shuttle utilizing laser-induced fluorescence techniques was investigated. A feasibility study of LIDAR (Light Detection and Ranging) techniques to detect twelve gases of scientific and military interest was carried out. Evaluation of a European Space Agency LIDAR hardware design was also a task. The main emphasis was on determination of background noise, spectral transitions, atmospheric transmission and molecular absorption cross-section of the target in order to determine the minimum target concentration required to be detectable. Atomic sodium, molecular iodine and hydrogen flouride were determined to be promising candidates for LIDAR resonance detection. Other molecules investigated, such as hydrogen chloride, xenon and krypton were considered marginally detectable at best because of their small absorption cross-sections. Lack of sufficient data prevented extended analysis of the remaining molecules.

Contents

I. Introduction

In recent years, LIDAR (light detection and ranging) has become a valuable tool in remote sensing of atoms and molecules in the environment. With the introduction of tunable dye lasers, it has become possible to excite certain molecular resonances of atoms or molecules (hereafter referred to as particles) and monitor their emission to detmine their existance, concentration, and spatial extent in the region being investigated. In many instances, particular areas to be probed are virtually inaccessible to researchers because of their remoteness of location or their location in hostile countries. In these types of scenarios, LIDAR monitoring has the potential to obtain the information. Other techniques exist such as passive infrared spectrometry that can at times collect the same data using better developed technology. The advantage that the LIDAR has, however, is that it can, in certain instances, detect much smaller concentrations of a particular particle. The laser's narrow spectral linewidth allows one to excite and monitor a very small spectral interval and hence minimize unwanted background from reflected and atmospheric emissions. With the advent of the space shuttle, a new dimension in LIDAR remote sensing is available. Virtually any part of the world, any country, friend, or foe can be surveyed within minutes or a few hours for certain types of particles to obtain a deeper insight into natural processes or a country's commercial or military intentions.

Several important issues must be addressed, however, before this space-borne concept can become reality. Are tunable lasers available that are powerful enough to excite molecules hundreds of kilometers away, and is the fluorescence return of the molecules strong enough to

be detected over the sometimes overwhelming noise background? Can a laser beam remain relatively collimated at great distances so that all of the laser photons are placed at the point of interest? What is the atmospheric transmission of laser and fluorescence radiation? Lastly, and most importantly, how well do atoms and molecules of interest absorb and emit radiation?

The purpose of this thesis is to perform a feasibility study on the use of fluorescent LIDAR techniques from the space shuttle to detect several candidate atoms and molecules of scientific and military interest (see Table I). A European Space Agency LIDAR design was also evaluated.

Table I

Candidate Molecules for Investigation

Molecule	Reason for Interest
1. Sodium	Prove/disprove theory of thunderstorm updraft as a source of upper atmospheric sodium.
2. HCl	
3. HF	
4. B_2O_3	Possible by-products in rocket engine combustion.
5. HBO_2	
6. Al_2O_3	
7. H_2	
8. HT	Possible by-products from a nuclear facility.
9. HTO	
10. I_2	By-product isotopes from a nuclear explosion.
11. Xe	
12. Kr	

II. Theory

The Basic LIDAR Equation

LIDAR resonance fluorescence involves laser excitation of a resonance line in an atom or molecule followed by detection of photons created by spontaneous radiative decay. The wavelength of the fluorescent photons can indicate the exact species emitting. For a given scenario, it is imperative that a sufficient number of photons reaching the detector be distinguished from the background and detector noise. The available number of absorbing particles is given by

$$K = a\int n'(Z)dZ$$

where:

a = area of laser beam coverage at target

n'(Z) = number density of absorbers at an altitude Z residing in the proper energy state for laser beam absorption. This integral is known as the column density and has units of (length^{-2}).

The area (a) of laser beam coverage is governed by the beam divergence (Θ_D) of the laser (see equation 35). In order to minimize noise, the field of view (FOV) of the LIDAR receiver is matched to the beam divergence.

The limits on the above integral are governed by the sample time (Δt) and delay time (t_d). These will be defined later. The number of photons per unit area incident at the region of interest is given by:

$$\text{photons per unit area incident} = \frac{I}{a}$$

assuming a uniform beam.

where:

I = total number of photons incident at the target. The total number of photons absorbed is given by:

Total Number Absorbed = $IK\sigma$

where:

σ = effective absorption cross-section

This assumes an optically thick target, i.e. $n'\sigma\Delta Z<<1$ where ΔZ is the path length of absorbers.

The number of photons radiated per unit solid angle is equal to the number absorbed divided by 4π steradians. The number of photons actually reaching the receiver in the absence of atmospheric transmission losses is equal to the number emitted into the solid angle subtended by the receiver aperture:

$$\text{Photons reaching receiver} = \frac{IK\sigma A}{4\pi Z^2}$$

where

Z = range between cloud and receiver

A = area of receiver aperture

The actual number of photons detected is determined by three other factors: detector quantum efficiency (η), fluorescence efficienty (0_F) and receiver throughput efficiency (ε). Atmospheric transmission losses result from fluorescence emission being absorbed and scattered by other particles in the atmosphere. If the laser is at a different wavelength than the fluorescence, then the loss factor is given as the product of the transmitted laser beam losses (T_t) and the received signal losses (T_R). Detector quantum efficiency is the number of electrons produced per incoming photon.

The value for η is usually 10% - 20% for detectors in visible or infared. Fluorescence efficiency, or branching ratio, is the ratio of the number of transitions that occur from upper level (a) to a lower

level (b) to the number that decay from level (a) to all possible lower levels. Receiver throughput efficiency accounts for losses in reflection off mirrors and transmission through filters and windows. With the above factors included, one can now write the general LIDAR equation relating the number of signal photons detected per sample time to the various parameters of range, laser size, etc:

$$N = \frac{IK\sigma\Lambda\varepsilon\eta O_F T_R T_t}{4\pi Z^2} \qquad (1)$$

This equation assumes that the emitted laser pulse and the fluorescence lifetime (τ) of the target are short compared to the integration time (Δt) of the detector. Of the molecules considered in this thesis, this was not always the case, thus a modified form of the LIDAR equation was developed by the author. The expression for the modified LIDAR equation will be derived later.

It should be noted that in most cases the column density (K) is expressed as the product of an average target number density (n') and column length being sampled (ΔZ). The column length being sampled can be related to the sample time by the relationship:

$$\Delta Z = \frac{1}{2} c \Delta t \qquad (2)$$

where:

c = speed of light

The longer the detector samples the fluorescence return, the larger is the column being sampled.

The particular region in the atmosphere where sampling occurs is governed by the delay time (t_d) between laser pulse and initilization of detector sampling (see fig 1). For the case where the shuttle LIDAR is viewing straight down at the earth, if t_d is increased, then the

region being sampled is farther away from the shuttle and thus closer to the earth. As t_d is shortened, then sampling occurs closer and closer to the shuttle. In short, the sample time (Δt) specifies the column length being sampled while the delay time (t_d) fixes the distance between receiver and sampling region. Extending Δt, to increase the number of photons returned can be done only to a certain point. If the cloud of interest is highly localized then there is a fixed ΔZ where molecules of interest reside and one must adjust Δt by equation (2) to obtain the optimum return. This statement is always true if the radiative decay time (τ) is much shorter than Δt. If it is not, then it may be advisable to extend Δt farther to allow detection of photons from late-decaying particles but short enough to avoid additional noise from reflected laser light off of the earth.

The total time from the first laser pulse to the last fluorescence sampling is known as τ_d (see fig 1). If a LIDAR "sounding" period is very long ($\tau_d \tilde{\simeq} 10$ seconds) then look angle and range can no longer be treated as constants and equation (1) must be modified (see fig 2). This scenario can get very complicated thus this thesis will be restricted to short τ_d.

Atmospheric Transmittance

The coefficient of transmission through a slab (ΔL) of atmosphere is defined as (ref 1:10):

$$T_{SLAB} = \exp(-\gamma \Delta L) \qquad (3)$$

where:

$$\gamma = S_m + S_a + K_m + K_a \qquad (4)$$

and

S_m = Molecular scattering (Rayleigh)

S_a = Aerosol scattering (Mie)

K_m = Molecular absorption (resonance)

K_a = Aerosol absorption

Rayleigh scattering takes place between a photon and an atom or molecule whose size is smaller than the wavelength (λ) of the photon. It's cross-section has a λ^{-4} dependence. Mie scattering is much more complex and involves scattering of a photon off of a particle comparable in size with the wavelength of the light. The γ coefficient is a function of altitude and wavelength. Using the tables for laser line transmittance (ref 1:17,18), one can determine the total transmittance through many slabs of atmosphere by the product of equation (3) for each slab (ref 1:12);

$$T_{TOT} = T = \exp\left(-\sum_j \gamma_j \Delta L_j\right) \qquad (5)$$

These tables did not list the desired laser wavelengths used in this study, however it is appropriate to interpolate between two wavelength values for K_a, S_m and S_a because they are slowly varying functions. This is not the case at all for K_m which is a highly oscillatory function of wavelength. Fortunately in this thesis the number density of abosrbers at the wavelengths of interest are low enough to allow K_m to be discarded.

Modified Forms of the Basic LIDAR Equation

For other than vertical sounding, the look angle (θ) and range (Z) will be larger than zero degrees and Z_v respectively (see fig 1). This may happen frequently when the shuttle's orbital parth does not take the LIDAR directly over the event of interest. The transmission co-

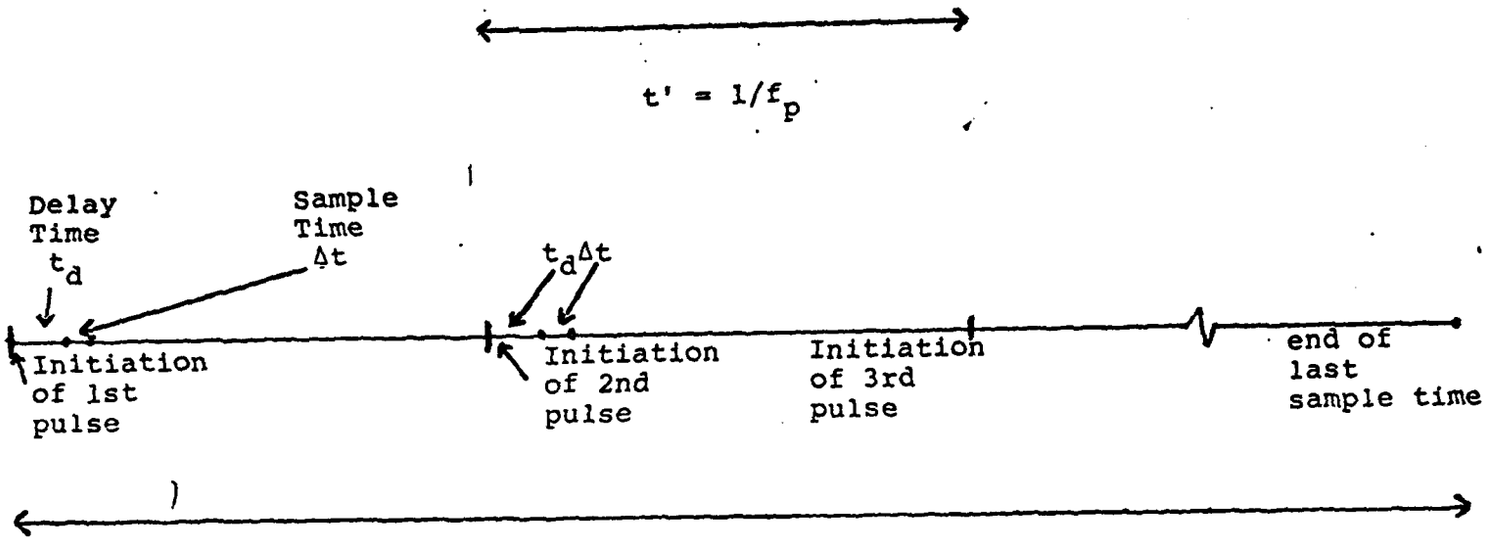

Figure 1. LIDAR Sounding timeline

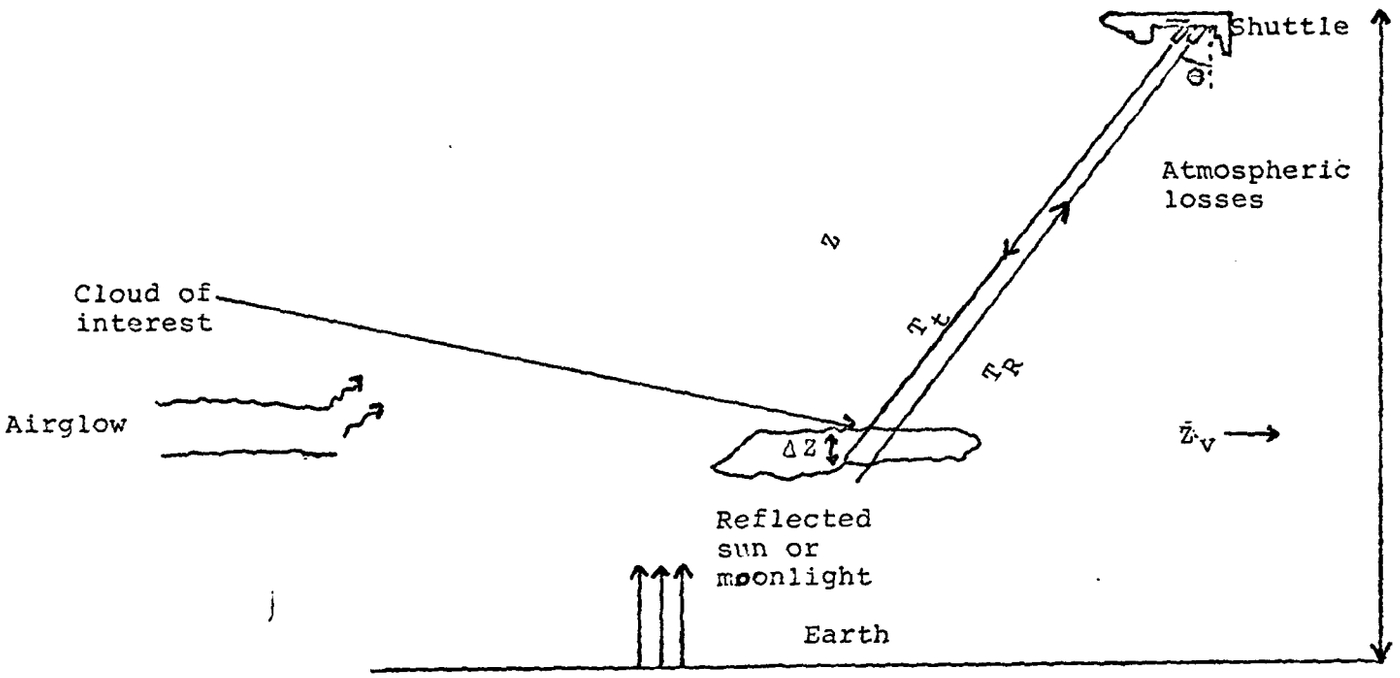

Figure 2. Shuttle LIDAR Scenario

efficients (T_t) and (T_R) will take the form:

$$T(\Theta,\lambda) = \exp\left(-\sum_j \gamma_j \Delta L_j\right)^{\sec \Theta} \quad (6)$$

or:

$$T(\Theta,\lambda) = T^{\sec \Theta} \quad (7)$$

Where T is given by equation (5). The range at angle Θ is given by the relationship

$$Z = Z_v \sec \Theta \quad (8)$$

where:

Z_v = nadir range (see fig 2)

For a sounding about a region other than nadir, equation (1) becomes:

$$N = \frac{IK\sigma A\epsilon\eta\Theta_F (T_R T_t)^{\sec \Theta}}{4\pi Z_V^2 \sec^2 \Theta} \quad (9)$$

To repeat, it is assumed that τ_d is short so that Θ and Z can be treated as constants. Also Θ is assumed small in order to use a flat earth atmosphere geometry.

Equation (1) assumed that the lifetime of the state (τ) was very short compared to the sample time (Δt) of the fluorescence received by the detector. This meant that it was safe to assume that all of the fluorescence photons from the target emitted in the narrow solid angle of the detector are collected assuming that†

$$t_d = 2Z/c \quad (10)$$

If the lifetime (τ) is longer or comparable to the sample time(Δt) then the detector will not collect all of the emitted photons but, in many

†The proper delay time assures that no photons emitted into the detector field of view are missed and at the same time minimizes background noise by keeping Δt as small as possible.

cases only a small fraction of them in a sample time. If the lifetime is long enough, it is possible, in a later sample time, to continue receiving photons from particles excited many pulses ago and just beginning to decay. The total number of photons absorbed per pulse, ignoring transmission losses for the present time, is given by:

$$N_{ABS} = IK\sigma$$

where:

I = number of photons per laser pulse

The total number of photons decaying after the first laser pulse in a time interval (Δt) is given as:

$$N_{\text{decay 1}} = N_{ABS} - N_{ABS}e^{-A^*\Delta t}$$

where the factor $N_{ABS}e^{-A^*\Delta t}$ represents the number of particles still excited after a time interval (Δt). (A^*) is the sum of the Einstein coefficient for spontaneous radiative transitions between the excited and ground states and a deexcitation collision frequency. During the second pulse period, the number of photons absorbed will be the same as in the first pulse period (assuming that the laser output is the same for each pulse). The number of photons decaying during the second sample time (Δt) after the second laser pulse will be equal to:

$$N_{\text{decay 2}} = \underbrace{(N_{ABS}}_{\substack{\text{2nd}\\\text{pulse}}} - \underbrace{N_{ABS}e^{-A^*\Delta t})}_{\substack{\text{2nd}\\\text{pulse}}} + \underbrace{N_{\text{decay}}}_{\substack{\text{Leftover}\\\text{1st pulse}}}$$

The number of molecules decaying during the second sample time will be from some molecules excited during the second pulse plus some left over from the first pulse that are just beginning to deexcite. This second terms is equal to:

$$N'(1 - e^{-A^*\Delta t})$$

Where N' is the number of excited molecules left over from the first

pulse that are still in the excited state when the second pulse is occuring. If a laser has a pulse repetition frequency of f_p hertz, then the time between pulses (t') is equal to $1/f_p$. This is the amount of time elapsed between laser pulses and represents the amount of time that the first group of excited particles has had to decay. Therefore, the number of excited molecules left over the from the first pulse at the beginning of the second sampling time is:

$$N' = \underset{\substack{\text{1st}\\\text{pulse}}}{N_{ABS}} e^{-A^*t'} = \underset{\substack{\text{1st}\\\text{pulse}}}{N_{ABS}} e^{(-t'/\tau_R + \tau_c)}$$

Where $\tau_R + \tau_c$ represent respectively the radiative lifetime of the molecule and the time between collisions. If all laser pulses are equal then N_{ABS} for all pulses are the same. The total number of decaying events during the second sample time (Δt) is then:

$$N_{decay\ 2} = N_{ABS}\ (1 - e^{-A^*\Delta t}) + N_{ABS} e^{-A^*t'}\ (1 - e^{-A^*\Delta t})$$

$$N_{decay\ 2} = N_{ABS}\ (1 - e^{-A^*\Delta t})\ (1 + e^{-A^*t'})$$

It is easy to see that during the third sample time, the decaying particles will come from molecules excited from the third laser pulse in addition to some left over from the second and first pulses:

$$N_{decay\ 3} = N_{ABS}\ (1 - e^{-A^*\Delta t}) + N_{ABS} e^{-A^*t'}\ (1 - e^{-A^*\Delta t})$$

$$+ N_{ABS} e^{-2A^*t'}\ (1 - e^{-A^*\Delta t})$$

Simplifying, we have:

$$N_{decay\ 3} = N_{ABS}\ (1 - e^{-A^*\Delta t})\ (1 + e^{-A^*t'} + e^{-2A^*t'})$$

The number decaying in the Nth pulse is given by:

$$N_{\text{decay } N} = N_{ABS}\,(1 - e^{-A^*\Delta t})\,(1 + e^{-A^*t'} + e^{-2A^*t'} + \ldots + e^{-(N-1)A^*t'})$$

or:

$$N_{\text{decay } N} = N_{ABS}\,(1-e^{-A^*\Delta t}) \sum_{J=0}^{N-1} e^{-JA^*t'}$$

The total number of deexcited molecules after N sample times is given by:

$$N_{\substack{\text{decay} \\ \text{Total}}} = N_{\text{decay } 1} + N_{\text{decay } 2} \cdots + N_{\text{decay } N}$$

A little thought will reveal that this expression can be written as:

$$N_{\substack{\text{decay} \\ \text{Total}}} = \sum_{i=0}^{N-1} N_{ABS}\,(1-e^{-A^*\Delta t}) \sum_{J=0}^{i} e^{-JA^*t'}$$

This can be written more explicitly in the following way:

$$N_{\substack{\text{decay} \\ \text{Total}}} = IK\sigma\,(1-e^{-A^*\Delta t}) \sum_{i=0}^{N-1} \sum_{J=0}^{i} e^{-JA^*/f_p} \qquad (11)$$

If the product A*t' is much less than 1, we may expand the exponential in a Taylor series keeping only the first two terms:

$$e^{-JA^*t'} = (e^{-A^*t'})^{J} = (1-A^*t')^{J} \qquad (12)$$

and if $A^*\Delta t$ in equation (11) is small compared to 1, which is usually the case, we may say:

$$1-e^{-A^*\Delta t} = A^*\Delta t \qquad (13)$$

With the above approximations, we can simplify equation (11) to read:

$$N_{\substack{\text{decay} \\ \text{Total}}} = IK\sigma A^*\Delta t \sum_{l=0}^{N-1} \sum_{J=0}^{i} (1-A^*/f_p)^{J}$$

The total number of photons actually detected by the LIDAR receiver over N sample times is given as:

$$N_{\substack{\text{Tot} \\ \text{Detect}}} = \frac{n_R}{n_T} \frac{Ik\sigma\,(1-e^{-A^*\Delta t})\,T_r T_t A\eta\varepsilon\Theta_F \sum_{i=0}^{N-1} \sum_{J=0}^{i} e^{-JA^*/f_p}}{4\pi Z^2}$$

The factor (n_R/n_T) will be discussed shortly.

Finally, the most general case considers look angle dependence. Recalling equations (7), (8) and (9) we have:

$$N_{\substack{\text{Total}\\\text{Detect}}} = \frac{n_R}{n_T} \frac{IK\sigma(1-e^{-A^*\Delta t})A\eta\varepsilon\Theta_F (T_R T_t) \sec\Theta \sum_{i=0}^{N-1} \sum_{J=0}^{i} e^{-JA^*/f_p}}{4\pi Z_v^2 \sec^2\Theta} \quad (14)$$

If the conditions outlined by equations (12) and (13) hold true, we may rewrite equation (14) as:

$$N_{\substack{\text{Total}\\\text{Detect}}} = \frac{n_R}{n_T} \frac{IK\sigma A^*\Delta t A\eta\varepsilon\Theta_F (T_R T_t)^{\sec\Theta} \sum_{i=0}^{N-1} \sum_{J=0}^{i} (1-A^*/f_p)^J}{4\pi Z_v^2 \sec^2\Theta} \quad (15)$$

Quenching

The factor (n_R/n_T) occurs because only a fraction of decaying molecules decay radiatively. Others decay non-radiative by through collisional deexcitation with other molecules. This process is known as quenching. Quenching, or non-radiative deexcitation, as it is sometimes called can result in a reduction in photon return if the time between collisions of molecules is comparable to, or smaller than the radiative lifetime of the state. Using the relationship:

$$\frac{1}{2} M\langle u\rangle^2 = \frac{3}{2} kT \quad (16)$$

for a gas in equilibrium, one can solve for the velocity of the molecules. The time between collisions is equal to the mean free path between collisions divided by the velocity of the molecules:

$$\tau_c = \frac{\lambda}{\langle u\rangle} = \frac{1}{n_c \sigma_c \langle u\rangle} \quad (17)$$

where:

n_c = Total number density of all molecules present.

$\sigma_c = 10^{-15}$ cm^2 (collisional cross-section for quenching). (ref 22:4217)

The question now is: in a sample time (Δt), how many excited molecules will decay through radiative processes relative to the total number that decay through both radiative and collisional processes? For a total number (n) of excited molecules, the decrease of n in a time (dt) is given by:

$$-dn = dn_R + dn_C \tag{18}$$

where:

$$dn_c = ndt/\tau_c$$

and:

$$dn_R = ndt/\tau_R \tag{19}$$

By integrating over the sample time, one can obtain the total number of molecules remaining in the excited state after a time t:

$$dn = n\left(\frac{1}{\tau_R} + \frac{1}{\tau_C}\right) dt = \alpha n dt$$

$$\int_{n_o}^{n} \frac{dn}{n} = \int_{o}^{t} -\alpha dt$$

$$\ln \frac{n}{n_o} = -\alpha t$$

which yields:

$$n = n_o e^{-\alpha t} \tag{20}$$

The total number that have undergone a transition (n_T) in time t is just equal to (n_o-n):

$$n_T = n_o\,(1-e^{-\alpha \Delta t})$$

The number of molecules which undergo a radiative transition in a time (dt) are given by equation (19). Using equation (20), equation (19) can be written as:

$$dn_R = \frac{n_o e^{-\alpha t}\, dt}{\tau_R} \qquad (21)$$

By integrating this expression over time, the total number of radiative transitions in Δt can be obtained: Integrating, we have:

$$\int_o^{n_R} dn_R = \frac{n_o}{\tau_R} \int_o^t e^{-\alpha t}\, dt$$

which yields:

$$n_R = \frac{n_o}{\alpha \tau_R} \quad 1-e^{-\alpha \Delta t} \qquad (22)$$

In a time (Δt), the fraction that have undergone a radiative decay is given by:

$$\frac{n_R}{n_T} = \frac{n_o \quad 1-e^{-\alpha \Delta t}}{\alpha \tau_R n_o \quad 1- \quad -\alpha \Delta t} = \frac{1}{\alpha \tau_R}$$

This can be written more explicitly as:

$$\frac{n_R}{n_T} = \frac{1}{1 + \frac{\tau_R}{\tau_C}} \qquad (23)$$

From this expression, it is easy to see that as collisions become dominant (τ_c decreasing) then n_R/n_T decreases and visa versa. If there are no appricable collisional effects, than $\tau_R/\tau_C \to 0$ and $n_R/n_T \to 1$ as expected. This just says that all transitions are radiative ones.

Effective Cross-Section

The cross-section (σ) used in this thesis is an effective cross-section for the absorptance of a doppler-broadened particle given a doppler broadened laser line. The absorption line profile of the particle is given as:

$$\sigma(\nu) = \frac{2\sigma_o (\ln 2)^{\frac{1}{2}}}{\pi^{\frac{1}{2}}\Delta\nu_D} \exp \frac{-4(\ln 2)(\nu-\nu_o)^2}{\Delta\nu_D} \qquad (24)$$

where (ref 2:65):

$$\sigma_0 = \frac{e^2 f}{4\varepsilon_0 M_e C} \quad \text{(For atomic particles)}$$

$\Delta\nu_D$ = linewidth at full width half maximum

e = electron charge

f = oscillator strength

ε_o = permittivity of free space

M_e = electron mass

For molecules another form of σ_o is used (ref 3):

$$\sigma_o = \frac{g_a A' \lambda^2_{ab}}{g_a 8\pi} \quad \text{(For molecules)} \qquad (26)$$

where:

g_a = degeneracy of level (a)

g_b = degeneracy of level (b)

A' = Einstein coefficient for spontaneous transition between levels (a) and (b).

λ_{ab} = wavelength of the transition

and finally:

$$\Delta\nu_D = 2\nu_o \frac{2KT}{MC^2} (\ln 2)^{\frac{1}{2}} \qquad (27)$$

where:

K = Boltzman's constant

T = temperature

M = mass of particle

ν_o = line center frequency

The laser lineshape profile is similar to equation (24):

$$L(\nu) = \frac{2(\ln 2)^{\frac{1}{2}}}{\pi^{\frac{1}{2}}\Delta\nu_L} \exp \frac{-4(\ln 2)\ (\nu-\nu_o)^2}{\Delta\nu_L}$$

Note that $L(\nu)$, unlike $\sigma(\nu)$, is a distribution function. This is because the magnitude of the laser energy (I) is explicitly expressed in equation (1). The laser linewidth ($\Delta\nu_L$) takes the same form as equation (27) but with different (T) and (M) values. In this thesis, a typical laser linewidth is assumed and not calculated. The effective cross-section is a convolution of the absorption and laser line profiles over all ν:

$$\sigma_{eff} = \sigma = \int_{-\infty}^{+\infty} L(\nu)\ \sigma(\nu)\ d\nu$$

$$\sigma = \frac{\sigma_o 4\ln 2}{\pi\Delta\nu_L\Delta\nu_D} \int_{-\infty}^{+\infty} \exp\ -4\ln 2\ (\nu-\nu_o)^2 \left(\frac{1}{\Delta\nu_L^2} + \frac{1}{\Delta\nu_D^2}\right) d\nu \qquad (28)$$

The integral has the form:

$$\int_{-\infty}^{\infty} e^{-a^2y^2}\ dy = \frac{\pi}{a}$$

Letting:

$$a = 4\ln 2\left(\frac{1}{\Delta\nu_L^2} + \frac{1}{\Delta\nu_D^2}\right)^{\frac{1}{2}}$$

equation (26) can be written as:

$$\sigma = \frac{\sigma_o 4(\ln 2)\pi^{\frac{1}{2}}}{\pi\Delta\nu_L\Delta\nu_D a}$$

This reduces to:

$$\sigma = \frac{2\sigma_o(\ln 2)^{\frac{1}{2}}}{\pi^{\frac{1}{2}}\Delta\nu_L\Delta\nu_D\left(\frac{1}{\Delta\nu_L^2} + \frac{1}{\Delta\nu_D^2}\right)^{\frac{1}{2}}} \qquad (29)$$

In many cases:

$$\Delta\nu_L >> \Delta\nu_D$$

therefore:

$$\left(\frac{1}{\Delta\nu_L^2} + \frac{1}{\Delta\nu_D^2}\right)^{\frac{1}{2}} = \frac{1}{\Delta\nu_D}$$

Plugging this into equation (29) we obtain:

$$\sigma = \frac{2\sigma_o (\ln 2)^{\frac{1}{2}}}{\pi^{\frac{1}{2}} \Delta\nu_L} \qquad (30)$$

Noise

Noise can enter the system in a variety of ways. Earth-reflected sun, moon, and laser light all result in unwanted photons reaching the detector. These photons along with detector and signal noise place a lower limit on the number of signal photons (N) that must be counted or detected in a given sample time. This then places a lower limit on the column density (K) of absorbers required through equation (1). The photons arriving at the detector are generated from random processes, therefore they obey poisson statistics. The probability that m photons will arrive in time t is given by:

$$P(m,t) = \frac{(I_p t)^n}{m!} \exp(-I_p t) \qquad (31)$$

where:

I_p = average rate of photon arrival

From the poisson distribution, the average number of photons ($\bar{m}$) arriving in a time t is given by $I_p t$ and the variance in m is given by $I_p t$. The signal to noise ratio is given by:

$$\frac{S}{N} = \frac{\bar{m}}{\sigma_p} = \frac{I_p t}{(I_p t)^{\frac{1}{2}}} = (I_p t)^{\frac{1}{2}} = \bar{m} \qquad (32)$$

where:

σ_p = square root of the varience

The above expression considers noise only as a result of the random arrival of signal photons. The value σ_p however must include further noise contributions from the sources mentioned above. When these are included we have:

$$\sigma_p = (Nf_p\tau_d + N_E\tau_d f_p + N_M\tau_d f_p + N_A\tau_d f_p + N_d\tau_d f_p)^{\frac{1}{2}} \qquad (33)$$

where:

f_p = pulse repetition frequency

τ_d = total sounding time

N = average number of signal photons counted per sample time (equation 1)

N_E = average number of photons counted from earth-reflected sunlight per sample time.

N_M = average number of photons counted from earth reflected moonlight per sample time.

N_A = average number of photons per sample time counted from airglow in the atmosphere (sodium case only)

N_d = average number of thermal electrons created per sample time.

It is clear that the product $(f_p\tau_d)$ yields the total number of pulses or sample periods (Δt) taken in the total sounding period (τ_d). Therefore, the product of N, N_E, N_M, N_A and N_d with $f_p\tau_d$ yield a total number of photons collected in the sounding period (τ_d). Dark current results from thermally emitted electrons from the photocathode of a photomultiplier tube. The rate of electron emission per unit area is given by the Richardson equation (ref 9):

$$i_d = 120T^2 \exp\left(\frac{-1.16X10^4\psi}{T}\right)\left(\frac{\text{amperes}}{\text{cm}^2}\right) \qquad (34)$$

where:

T = temperature (^oK)

ψ = work function of the photocathode material (ev). The amount of current is proportional to the area of the photocathode. Finally, we have:

$$N_d = (i_d \frac{\text{coulomb}}{\text{sec cm}^2})\ (6.25X10^{18} \frac{\text{electrons}}{\text{coulomb}})(A_{pc}\ \text{cm}^2)\ (\Delta t\ \text{sec}) \qquad (35)$$

where:

A_{PC} = Photocathode area

If the photocathode is cooled, it is possible to reduce N_d to a negligible level and thus eliminate it from the signal to noise calculations.

In the case of a photomultiplier tube, a further contributor to noise is from the individual dynodes in the amplifying chain. This factor, along with equations (32) and (33) yield the final expression for signal to noise:

$$\frac{S}{N} = R = \frac{Nf_p\tau_d(\frac{\delta-1}{\delta})^{\frac{1}{2}}}{(Nf_p\tau_d+N_Ef_p\tau_d+N_Mf_p\tau_d+N_Af_p\tau_d+N_df_p\tau_d)^{\frac{1}{2}}}$$

or:

$$R = \frac{N(f_p\tau_d)^{\frac{1}{2}}\ (\frac{\delta-1}{\delta})^{\frac{1}{2}}}{(N+N_E+N_M+N_A+N_d)^{\frac{1}{2}}} \qquad (36)$$

where:

δ = gain of individual dynode in photomultiplier.

Of course, if some detector other than a photomultiplier is used, the factor $(\frac{\delta-1}{\delta})^{\frac{1}{2}}$ is not used in equation (36). Also, if the detector temperature is lowered enough, N_d can be neglected. Lastly, N_A will only occur when sodium LIDAR soundings are considered.

Values for N_E and N_M are derived from a radiance vs. wavelength chart (ref 4:42). The radiance (L) for a body is the number of photons

per second per unit area per steradian emitted in a wavelength interval ($\Delta\lambda$). The total number of photons detected in a sample time (Δt) is given by the product:

$$La\Omega(\Delta\lambda)\ (\Delta t)\eta\epsilon \tag{37}$$

where:

a = area of source observed

Ω = solid angle subtended by the receiver

$\Delta\lambda$ = wavelength interval sampled

The observed source area (a) is determined by the field of view (FOV) of the detector. For a FOV of Θ_D the area (a) is given by:

$$a = \pi r^2 = \frac{\pi\Theta_D^2 z^2}{4} \tag{38}$$

The solid angle subtended by receiver with aperture area (A) is given as:

$$\Omega = \frac{A}{z^2} \tag{39}$$

Combining equations (37), (38) and (39) we have:

$$N = \frac{LA\pi\Theta_D^2\eta\epsilon\Delta\lambda\Delta t}{4} \quad \frac{\text{photons detected}}{\text{sample time}} \tag{40}$$

The wavelength interval ($\Delta\lambda$) sampled is governed primarily by the band-pass filter used in the receiver. Usually, to avoid as much background as possible a Fabry-Perot etalon is placed in the system to achieve very narrow (angstrom) bandpass windows. The values for L in (ref 3:1710) are for a specific case:

$$\Delta t = 6.6\ \mu\text{sec}$$

and

$$T_R T_t = .5$$

In order to obtain a general radiance simply multiply the radiance values in reference (3) by 2 and divide by 6.6 μsec.

Equation (36) can be solved for the minimum number of signal photons required per sample time to achieve a signal to noise ratio (R). Squaring both sides of equation (36) we obtain:

$$R^2 = \frac{N^2 f_p \tau_d \ (\delta-1)}{(N+N_E+N_M+N_A+N_d)\delta}$$

Rearranging to a more familiar form we obtain:

$$f_p \tau_d \ N^2 + \frac{-R^2\delta}{(\delta-1)} N + \frac{-R^2\delta}{(\delta-1)} \ (N_E+N_M+N_A+N_d) = 0$$

This is a quadratic equation in N. Using the quadratic formula we obtain:

$$N_{min} = \frac{\frac{R^2\delta}{(\delta-1)} \pm \left[\frac{R^4\delta^2}{(\delta-1)^2} + \frac{4 f_p \tau_d R^2 \delta (N_E+N_M+N_A+N_d)}{(\delta-1)}\right]^{\frac{1}{2}}}{2 f_p \tau_d} \qquad (41)$$

The result of equation (41) can be substituted in for N in equation (1) and a minimum column density, (K) can be obtained for a given R.

Laser Beam Divergence

All of the LIDAR equations discussed so far have assumed that the area of the laser beam at the target is smaller than, or equal to the area of the cloud being investigated. If the laser beam were bigger, then many laser photons would never find a target particle and the return signal would be smaller. This could be disasterous in many sitatuions where LIDAR detection of various molecules is marginal at best. It is imperative, therefore to assure that the beam is always smaller than the target. This can be accomplished ironically, by initially expanding the beam at the laser transmitter. The full angle beam divergence is given from Fraunhofer diffraction theory to be:

$$\Theta_D = \frac{1.22\ \lambda}{D} \qquad (42)$$

where:

Θ_D = beam divergence in radians

D = diameter of laser beam exit aperture

For small beam divergences we may approximate the diameter (d) of the laser beam spot at a distance (Z) from the shuttle LIDAR platform by the relationship:

$$d = \Theta_D Z \qquad (43)$$

Using equation (42) we may rewrite equation (43) to directly relate aperture diameter, range and beam spot size:

$$D = \frac{1.22\lambda Z}{d} \qquad (44)$$

Range, laser wavelength and target extent will have to be evaluated for each scenario considered to determine if the laser on board the shuttle needs an expanding telescope or not.

III. LIDAR Conceptual Design

The LIDAR hardware consists of two main parts. The laser transmitter and receiver (fig 3). The laser transmitter in most cases is a tunable dye laser with expanding optics if needed. The receiver could be a Cassegrain telescope with folding mirrors to minimize the extent of the optical train (ref 5:191). In order to obtain a very narrow spectral window, (on the order of Angstroms or fractions of an angstrom), a Fabry-Perot or several Fabry-Perot etalons in series are used. In order to assure proper functioning of the etalons, a collimating lens is used ahead of the etalons. The transmitted signal through the etalon is then sent to a detector which may be a photomultiplier for detection of wavelengths in the visible and near IR or a photovoltaic detector for near and far IR photons. At the same time, an array of detectors is irradiated which allows determination of misalignment between laser and receiver. This information is sent to a processor which issues commands to activators to realign the two. The parameters ε and η deal with the losses through the receiver. These parameters are functions of wavelength; thus they will be computed for each molecule being investigated.

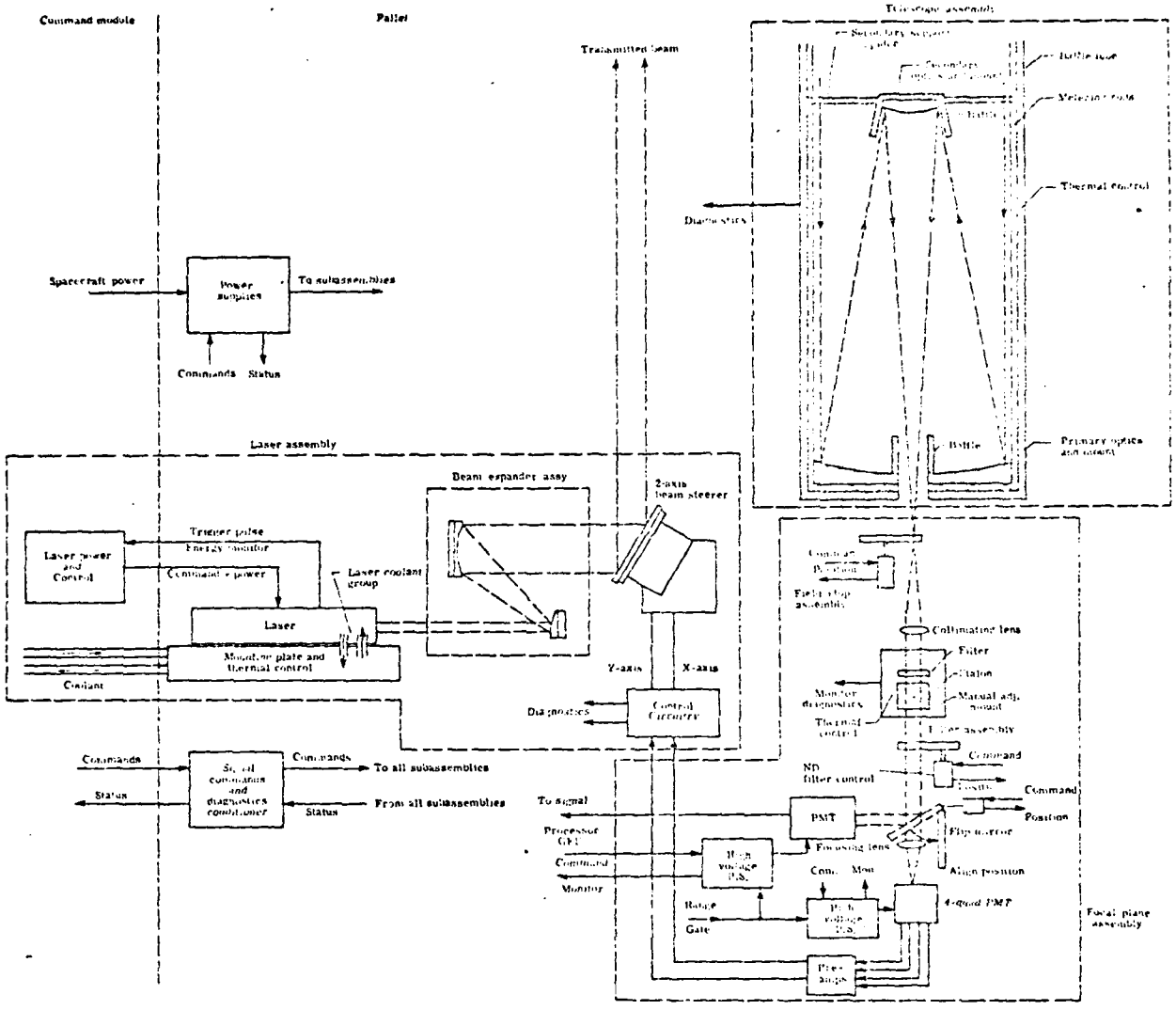

Figure 3. - Transmitter/receiver schematic of Perkin-Elmer Spacelab-lidar design.

IV. Molecules Investigated

A. Sodium

The sodium atom is of interest in this thesis for two reasons. First, it represents an interesting molecule for scientific reasons. There is more natural sodium in the atmosphere than expected. The question is, where does it come from? One theory is that it is coming from the salt water in the oceans and being drawn into the air by thunderstorm updrafts (ref 5:69). LIDAR soundings of thunderstorms should be able to detect this sodium thus proving or disproving the theory. Secondly, it allows a check of the results of this work with previous LIDAR sodium research (ref 6).

Transition

The (D_1) (5896Å) line of sodium was chosen as the wavelength to excite and detect the atoms. This electronic transition ($3^2S_{\frac{1}{2}} \rightarrow 3^2P_{\frac{1}{2}}$) is in the visible (yellow) region of the spectrum and well within the capability of the dye laser.

Effective Cross-Section

Assuming a sodium gas temperature of 300°K we can determine the doppler-broadened linewidth using equation (27) and the particular values for sodium:

$T = 300^{\circ}K$

$M = 23\ (AMU) \times 1.67 \times 10^{-27}\ kg/AMU = 8.834 \times 10^{-25}\ kg$

$$\nu_o = \frac{c}{\lambda_o} = \frac{2.998 \times 10^{10}\ cm/sec}{5896 \times 10^{-8}\ cm} = 5.0843 \times 10^{14}\ Hz$$

we obtain $\Delta\nu_o$ = (2.7341 X 10^8Hz). We choose a typical laser linewidth of 1Å (ref 7:350) which can be converted into frequency bandwidth for comparison with the sodium absorption linewidth ($\Delta\nu_D$) by the formula:

$$\Delta\nu = \frac{c}{\lambda^2}\Delta\lambda \qquad (45)$$

This gives:

$$\Delta\lambda_L = 8.6242 \text{ X } 10^{10} \text{ Hz} \qquad (46)$$

Since $\Delta\nu_L >> \Delta\nu_D$ we may use equations (25) and (30) to obtain an effective cross-section of:

$$\sigma = 1.01 \text{ X } 10^{-17} m^2 \qquad (47)$$

where the oscillator strength (f) is equal to (.33) (ref 26).

LIDAR Receiver Calculations

Assuming a LIDAR receiver design as in figure (4), we have reflectance losses from four mirrors, transmission losses through the collimating lens, etalon and photomultiplier tube window. At 5896Å, a silver coating appears to be the best reflector for the mirrors (ref 4:187) with a reflectance of (.98). The Fabry-Perot can be made 99% transmissive about a bandwidth ($\Delta\lambda$) of 1 angstrom. The collimating lens will normally lose 4% at each surface, so it should be about 92% transmissive. The RCA 7265 photomultiplier tube has a photocathode quantum efficiency of (.09) at 5896Å ((Cs)KNa_2Sb). An entrance window on the photomultiplier tube would have about a 92% transmission factor. The total throughput factor is then:

$$\epsilon\eta = (.98)^4(.99)^2(.92)^2(.09) = .06885 \qquad (48)$$

The diameter of the telescope primary mirror is initially chosen to be one meter in agreement with several LIDAR design studies. This gives:

$$A = .785\ m^2$$

for the area of the receiver aperature.

Fluorescence Efficiency

For the sodium D_1 line, the fluorescence efficiency (Θ_f) is equal to one. In other words, when the sodium atom is excited up to the $3^2P_{\frac{1}{2}}$ level, it can only decay back to ground state ($3^2S_{\frac{1}{2}}$) and no other.

Shuttle Altitude

The shuttle altitude is initially chosen to be 200km.

Laser Energy

The laser energy per pulse (I) is assumed to be one joule. This is an optimistic output energy for a dye laser of about an order of magnitude (ref 7:350).

Transmission Coefficients

Values of T_r and T_t as a function of penetration depth (χ) into the atmosphere are generated by interpolation between values for 5145Å and 6328Å, (ref 1:17,18). In this particular case, the laser and fluorescence wavelengths are the same, therefore:

$$T_r = T_t = T$$

Table II gives the transmission values for the sodium D_1 line. The penetration depth (χ) is defined as equal to zero at 100KM altitude and 100KM at ground level. As an example of how to use the chart, if one wanted to probe a region 70 kilometers above the earth from a shuttle platform, one would go to Table II and read off the value for a penetration depth into the atmosphere of 30 kilometers and thus T = .9991. Thus the total transmission would be $(.9991)^2 = (.9982)$.

Table II

Sodium D_1 Line Transmission vs. Penetration Depth

X(KM)	T	X(KM)	T
0	1.0	84	.9779
30	.9991	85	.9741
50	.9997	86	.9449
55	.9996	87	.9406
60	.9994	88	.9358
65	.9991	89	.9307
70	.9983	90	.9254
75	.9961	91	.9197
76	.9953	92	.9135
77	.9944	93	.9069
78	.9933	94	.8971
79	.9919	95	.8891
80	.9902	96	.8812
81	.9878	97	.8571
82	.9848	98	.8026
83	.9815	99	.6781
		100	.4323

Noise Analysis

By utilizing equation (41), the minimum number of signal photons needed for a given signal to noise ratio (R) can be obtained. For this value, equation (9) can be used to determine the minimum column density. Before using these equations, values for N_E,N_M,N_d and, in the sodium case, airglow (N_A), must be calculated. From reference (4:42), radiance values for reflected sunlight and moonlight off of the earth at 5896Å are given as:

$$L_E = 1.8182 \times 10^{17} \left(\frac{\text{photons}}{m^2 \text{str.Å sec}}\right)$$

and

$$L_M = 2.4242 \times 10^{11} \left(\frac{\text{photons}}{m^2 \text{str.Å sec}}\right)$$

The abbreviation (str.) stands for seradian. Sodium airglow in the atmosphere has a daylight emittance value of 20 kilo-Rayleighs† which is 20×10^{13} photons per square meter, and a nighttime emittance of 100 Rayleighs (10^{12} photons per square meter per second) (ref 8). The radiance (photons emitted for m^2 per sec per steradian) is given by the relationship:

$$L = \frac{M}{4\pi} \qquad (49)$$

where:

M = emittance (20 kilo-Rayleighs for sodium dayglow and 100 Rayleighs for nightglow)

The radiance (L) of the dayglow is then 1.592×10^{13} $(\frac{\text{photons}}{m^2 \text{str. sec}})$ and the radiance for nightglow is 7.958×10^{10} $(\frac{\text{photons}}{m^2 \text{str.}})$. The number of photons detected per sample time for each source of noise is found by plugging in the appropriate values in equation (40). In the case of N_E and N_M we have an additional factor due to the solar Fraunhofer line at 5896Å. This factor reduces N_E and N_M because less solar energy is emitted at the D_1 wavelength due to absorption in the sun's atmosphere. Reflected *moon*light is affected because that light ultimately comes from the sun. Using equation (40) with:

$A = .785\ M^2$ $\qquad \epsilon = .765$

$\Theta_D = 10^{-4}$ rad $\qquad \Delta\lambda = 1\text{Å}$

$\eta = .09$ $\qquad \Delta t = 6.6\ \mu\text{sec}$

$\delta = 3.38$

† One Rayleigh is defined as 10^{10} photons per m^2 per second.

and a 20% reduction due to Fraunhofer absorption for N_E and N_M we obtain:

$$N_E = 101.88 \text{ photons/sample time}$$

$$N_M = 1.36 \times 10^{-4} \text{ photons/sample time}$$

$$N_A = 4.46 \times 10^{-2} \text{ photons/sample time (day) and}$$

$$7.10 \times 10^{-5} \text{ photons/sample time (night)}$$

The dark current noises (N_d) can be obtained by evaluating the Richardson equation (34) and substituting the result into equation (35). The work function (ψ) of the RCA 7265 photocathode was obtained by determining where the response goes to zero on the response vs. wavelength curve (ref 10). This occurs at 8200Å. By using the relationship:

$$\psi(ev) = \frac{12395}{\lambda(\text{Å})} \qquad (50)$$

with λ = 8200Å, one obtains 1.51 electron volts for ψ. Assuming a photocathode cooled to 223°K and a photocathode area of (.785) cm^2 (1 cm. in diameter), we obtain 1.92×10^{-14} electrons per sample time for N_d. Therefore, dark current can be neglected. During daylight observations, it is clear that N_E dominates all other sources of noise. We may therefore neglect contributions of N_M and N_A in equation (41). Using equation (41), a table of N_{min} vs. R can be generated for daylight observations (Table IV). For night LIDAR soundings, $N_E = 0$ and N_M and N_A become the dominant noise sources. Dark current again can be ignored. Using equation (41) again, a table of N_{min} vs. R for night observations can be generated (Table V). Choosing R = 10, tables of minimum detectable column density (K) vs. range, look angle, laser power and atmospheric penetration (Tables VI thru IX), are presented.

Table IV

Daylight N_{min} vs. R - Sodium Case

N_{min}	R
3.88	1
7.90	2
16.39	4
45.80	10
109.61	20
149.32	25

Table V

Night N_{min} vs. R - Sodium Case

N_{min}	R
.181	1
.568	2
2.227	4
14.2	10
56.8	20
88.76	25

Table VI

Daylight Minimum Detectable Column Density vs. Laser Energy - Sodium

Energy/Pulse (Joules)	I (10^{16} photons/pulse)	K_{min} (10^{12} M^{-2})	n_{min} (10^{3} cm^{-3})
1	297	3.6	3.6
.8	238	4.5	4.5
.6	178	6.0	6.0
.4	119	9.0	9.0
.2	59	18.2	18.2
.1	30	35.9	35.9
.01	3	359.0	359.0
.002	.6	1790.0	1790.0
.001	.3	3590.0	3590.0

Δt = 6.6 μsec

ΔZ = 1KM

η = .09

Z = 100KM

$\Theta = 0^{o}$ (nadir)

R = 10

T^2 = .98

A = .785 M^2

σ = 1.01 X 10^{-17} M^2

ϵ = .765

Shuttle altitude = 200KM

Table VII

Nightime Minimum Detectable Column Density vs. Laser Energy - Sodium

Energy/Pulse (Joules)	I (10^{16} photons/pulse)	K_{min} (10^{12} M^{-2})	n_{min} (10^{3} cm^{-3})
1	297	1.1	1.12
.8	238	1.4	1.40
.6	178	1.9	1.87
.4	119	2.8	2.80
.2	59	5.7	5.65
.1	30	11.3	11.3
.01	3	113.0	113.0
.002	.6	565.0	565.0
.001	.3	1130.0	1130.0

Other parameters are the same as those for Table VI.

Table VIII

Daylight Minimum Detectable Column Density

vs. Range and Look Angle - Sodium Case

Z (KM)	Z_v (KM)	K_{min} ($10^{13} M^{-2}$)	$T^2 \sec\theta$	θ (Deg)	n_{min} ($10^4 cm^{-3}$)
200	200	7.7	.185	0	7.7
198	198	2.2	.640	0	2.2
196	196	1.8	.774	0	1.8
194	194	1.7	.810	0	1.7
187	187	1.4	.884	0	1.4
175	175	1.1	.980	0	1.1
150	150	.82	.980	0	.82
125	125	.57	.980	0	.57
100	100	.36	.980	0	.36
75	75	.20	1.0	0	.20
230.94	200	13.3	.142	30	13.3
228.63	198	3.1	.597	30	3.1
226.32	196	2.4	.744	30	2.4
224.01	194	2.3	.784	30	2.3
215.93	187	1.9	.867	30	1.9
202.07	175	1.5	.977	30	1.5
173.21	150	1.1	.977	30	1.1
144.34	125	.76	.977	30	.76
115.47	100	.49	.977	30	.49
86.60	75	.27	1.0	30	.27
282.84	200	31.0	.092	45	31.0
280.01	198	5.2	.532	45	5.2
277.18	196	3.9	.697	45	3.9
274.36	194	3.6	.742	45	3.6
264.46	187	3.0	.839	45	3.0
247.49	175	2.2	.972	45	2.2
212.13	150	1.6	.972	45	1.6
176.78	125	1.1	.972	45	1.1
141.42	100	.73	.972	45	.73
106.07	75	.40	1.0	45	.40

I = 1 joule/pulse

All other fixed parameters are the same as those at the bottom of Table VI.

Table IX

Nightime Minimum Detectable Column Density

vs. Range and Look Angle - Sodium Case

Z (KM)	Z_v (KM)	K_{min} ($10^{12}M^{-2}$)	$T^2 sec\Theta$	Θ (Deg)	n_{min} ($10^3 cm^{-3}$)
200	200	23.8	.185	0	23.8
198	198	6.8	.640	0	6.8
196	196	5.5	.774	0	5.5
194	194	5.1	.810	0	5.1
187	187	4.3	.884	0	4.3
175	175	3.4	.980	0	3.4
150	150	2.5	.980	0	2.5
125	125	1.8	.980	0	1.8
100	100	1.1	.980	0	1.1
75	75	6.2	1.0	0	6.2
230.94	200	41.2	.142	0	41.2
228.63	198	9.6	.597	0	9.6
226.32	196	7.6	.744	0	7.6
224.01	194	7.0	.784	30	7.0
215.93	187	5.9	.867	30	5.9
202.07	175	4.6	.977	30	4.6
173.21	150	3.4	.977	30	3.4
144.34	125	2.4	.977	30	2.4
115.47	100	1.5	.977	30	1.5
86.60	75	8.3	1.0	30	8.3
282.84	200	95.8	.092	45	95.8
280.01	198	16.2	.532	45	16.2
277.18	196	12.1	.697	45	12.1
274.36	194	11.2	.742	45	11.2
264.46	187	9.2	.839	45	9.2
247.49	175	6.9	.972	45	6.9
212.13	150	5.1	.972	45	5.1
176.78	125	3.5	.972	45	3.5
141.42	100	2.3	.972	45	2.3
106.07	75	1.2	1.0	45	1.2

All other parameters, same as Table VIII.

The minimum column density values given above are compatible with results obtained in ref 6. They detected a column density of 6 X $10^{13}M^{-2}$ using similar LIDAR equipment.

CW vs. Pulsed LIDAR Mode

An analysis was made to determine for a given scenario, which laser mode, CW (continuous wave) or pulsed gave the larger signal to noise (R) thus allowing detection of a smaller column density. The scenario involves a one second sounding of the atmosphere around nadir from a shuttle altitude of 200KM. A τ_d of one second was again chosen to allow holding Θ constant; thus a potentially complicated integration over angle is eliminated. From the data of Bowman (ref 6) it was determined that the bulk of natural sodium in the atmosphere lies between 80 - 100 KM altitude.

The total number of signal photons obtained in the CW case is given by equation (1) where I now becomes $I_o\tau_d$ where:

I_o = laser output power (1 watt)

τ_d = total sounding time (1 second)

and the integration of K is between 80 and 100 KM. We make the approximation that Z = 100 KM (dsitance from the shuttle to the midpoint of the cloud). From ref 6, the column density is found to be $6 \times 10^{13} M^{-2}$. Substituting in the values of K and Z and the other standard values used in Table VI we obtain:

$$N_{CW} = 640 \text{ photons/sec.}$$

For the pulsed mode, equation (1) is also used in its normal form. Choosing I = .1 joule per pulse, f_p = 10 Hz and Δt = 133 μsec to allow sampling of a 20 KM layer (equation 10), we obtain:

$$N_{pulsed} = 640 \text{ photons/total sounding time}$$

So, for the same amount of laser photons in both CW and pulsed cases, we obtain the same signal return. The signal-to-noise however will <u>not</u> be the same. During daylight observations, the number of noise

photons detected by the receiver is given by equation (40). The parameters are all the same as those used previously except that Δt is now equal to τ_d (1 second) for the CW case and 133 μsec for the pulsed case. This means that the noise level for CW will increase tremendously. Using equation (40) we have for CW:

$N_E = 1.57 \times 10^7$ photons

$N_M = 20.6$ photons

$N_A = 6757.6$ photons (dayglow)

$N_L = 9445$ photons

The last term N_L deals with the additional noise due to laser beam scattering off of the earth. From (ref 9) the irradience at the aperture of the receiver due to the emittance of a disk of luminance (L) of radius (a) at a distance (Z) away where $Z >> a$ is given by:

$$E = \pi L \frac{a^2}{Z^2} = M \frac{a^2}{Z^2} \qquad (51)$$

where:

E = irradiance $(\frac{\text{photons}}{M^2})$ at the receiver plane

M = emittance of the disk $(\frac{\text{photons}}{M^2})$

Recall that for a Lambertian source $\pi L = M$

The size of the disk is determined by the FOV of the detector (equation 43). With Z = 200 KM and $\Theta_D = 10^{-4}$ radians, we obtain a 10 meter spot radius. The emittance (M) of the disk is given by:

$$M = \frac{I_o T_t r}{\pi a^2} = 1.6257 \times 10^{14} \frac{\text{photons}}{M^2 \text{sec}}$$

where:

$$I_o = 1 \text{ watt} = 2.97 \times 10^{18} \text{ photons/sec @ } 5896\text{Å}^{o}$$

T_t = laser transmission loss from space to ground (.43)

r = earth albedo or reflectance coefficient (.04)

πa^2 = area of disk being illuminated.

The number of photons entering the receiver aperature per second is given by:

$$N = T_R \, E \, A = 5.4876 \times 10^{13} \text{ photons/sec}$$

where:

T_R = photon transmission from the earth back to the receiver (.43).

Finally the number actually detected in the one second sounding time is given by:

$$N_L = N\epsilon \, \eta \Delta t = 9445 \text{ photons}$$

It is clear that the signal to noise during daylight observations is given by:

$$R = \frac{N}{(N_E)^{\frac{1}{2}}} \qquad (52)$$

due to the overwhelming magnitude of earth reflected sunlight. This gives a signal to noise of (.163). For the pulsed case, Δt = 133 μsec, and thus the noise values will be considerably reduced:

$$N_E = 2037.6$$

$$N_M = .027$$

$$N_A = .899 \text{ (dayglow)}$$

Again, for daylight observations the signal to noise is given by equation (52):

$$R_{pulsed} = \frac{640}{(2037.6)^{\frac{1}{2}}} = 14.18$$

So in daylight work, the pulsed mode is the only mode that will work. For night observations (N_E=0) we have:

$$R_{cw} = \frac{N}{(N+N_L)^{\frac{1}{2}}} = \frac{640}{(640 + 9445)^{\frac{1}{2}}} = 6.37$$

The pulsed case yields:

$$R_{pulsed} \quad \frac{N}{(N)^{\frac{1}{2}}} = 25.3$$

The pulsed mode is still the better mode to use. It is clear that for nanosecond radiative lifetimes that the pulsed mode is far superior to the CW mode because all signal photons can be collected quickly thus cutting down on noise. For long radiative lifetimes, one may be forced to sample longer to get as many signal photons as possible, but this can probably only be done in a noise free environment.

Beam Divergence

A beam divergence of 10^{-4} rad was assumed for the laser and FOV of the receiver. The question now is: "Does the laser need expanding optics to reduce diffraction and thus beam divergence?" Using equations (43) and (44) we obtain a required exit aperature for the beam of 7.19 millimeters. Such a small size suggests that no expanding optics are necessary.

Sodium Conclusions

It appears that very small quantities of sodium (average number density of 10^4 particles per cm^3) can be detected with good signal to noise over large ranges and look angles. The main reason for sodium's easy detection is its large cross-section ($10^{-17} M^{-2}$). This situation unfortunately is the exception rather than the rule. Therefore minimum

detectable column densities for other particles will be higher, and in some cases much higher than sodium. It is also clear that pulsed sounding of the atmosphere is superior to CW due chiefly to the large reduction in noise in the pulsed mode.

B. Hydrogen Chloride (HCl)

Hydrogen chloride is of interest because it is a possible by-product of rocket fuel combustion. The detection of certain molecules in a rocket plume makes it possible to determine what kinds of fuels and oxidizers are being used in the rocket and this may allow one to ultimately predict the performance characteristics of the vehicle.

Transition

For a LIDAR sounding, excitation of an electronic transition would be the most desirable way to detect HCl because of the large associated cross-sections. Unfortunately, the excitation of an electronic transition in HCl cannot be accomplished, because the transition from the electronic ground state to the first excited state lies far out in the ultraviolet region of the spectrum. This is beyond the capabilities of a tunable laser. Thus one must be content in attempting to excite infrared vibrational-rotational levels. Excitation of the fundamental ($\nu''=0 \rightarrow \nu'=1$) and first overtone ($\nu''=0 \rightarrow \nu'=2$) vibrational bands cannot be done with a dye laser since these transitions lie too far into the IR, beyond 1.2 μm which is the long wavelength cutoff of the present dye laser. The second overtone vibrational transitions ($\nu''=0 \rightarrow \nu'=3$) does allow use of the dye laser because this transition occurs in the region of 1.2 μm. There are other lasers such as the optical parametric oscillators (OPO) (ref 11:257) that allow tunability out to 3.5 μm, however they are a factor of one thousand smaller in pulsed output energy and are not as well developed as the dye laser.

Rotational transitions for the ground and excited states must be selected next. It is desirable to excite the rotational level that has

the highest population at a temperature (T). This is given by, (ref 12:41)

$$J_{MAX} = \left(\frac{kT}{2hcB}\right)^{\frac{1}{2}} - \frac{1}{2} \qquad (53)$$

where:

k = Boltzman's constant = 1.38 X 10^{-16} erg/^{o}K

h = Planck's constant = 6.626 X 10^{-27}erg/sec

c = speed of light = 2.998 X 10^{10} cm/sec

B = rotational constant† = 10.5 cm^{-1}

Using a typical rocket plume temperature of 1500^{o}K (ref 13:352) and a B coefficient of 10.5 cm^{-1} for the HCl (ref 12:63), we have for equation (53):

$$J_{MAX} = 7$$

Therefore the transition to be excited is:

($\nu''=0, J''=7 \rightarrow \nu'=3, J'=8$)††. This is the R(7) line of the second overtone transition at ω = 8447.6582 cm^{-1} or λ = 1.1838 μm. It is desirable to detect a slightly different wavelength so that Mie scattering by particulates in the atmosphere and plume can be avoided. The transitions ($\nu'=3 \rightarrow \nu''=2$) would ideally be the most desirable vibrational transition to detect. It is in the far IR, but this presents no problem since many detectors work quite well in the IR. The problem lies in the lack of data on $\nu'=3 \rightarrow \nu''=2$ (hot band) transitions especially data that would allow one to calculate an effective cross-section. Therefore, even though $\Delta\nu=1$ or 2 transitions are more likely than $\Delta\nu=3$, the latter is

---

†The rotational constant is defined as: $h/8\pi^2Ic$ where I is the moment of inertia of the molecule.

†† Note the accepted notation of double prime refering to the lower state and single prime for the upper state.

chosen simply because data is available on this transition. The rotational transition ($J'=8 \rightarrow J''=9$) at $\lambda = 1.2202$ μm must be used because of the selection rule $J=\pm 1$ and because of the desire to transmit and receive at different wavelengths. All of the HCl molecules do not lie in the same excited state at a finite temperature. On the contrary, at rocket plume temperatures there are many occupied states. The higher the temperature the more states are occupied. It becomes important to know, therefore, how many molecules there are in the state that is to be excited relative to the total number of HCl molecules being irradiated. This requires the use of the Boltzman distribution and an evaluation of the partition functions for vibration and rotation. The Boltzman distribution may not be valid in a rocket plume since the exhaust gases are not in equilibruim. However, the only alternative is detailed accounting of all chemical reactions and many are not well understood. According to the Boltzman distribution, the ratio of the population of the ith state to that of the ground state (n_o) is given as:

$$\frac{n_i}{n_o} = \frac{g_i}{g_o} \exp\left(-\Delta E_i/KT\right) \tag{54}$$

In the case of rotational levels:

$$\Delta E_R = J(J+1)BhC \tag{55}$$

where:

J = rotational quantum number

g_i = degeneracy of the ith level = (2i+1)

B = rotational constant (for HCl) = 10.59 cm^{-1})

The ratio of interest is n_i/n_{TOT} where n_{TOT} represents the total number of molecules. The total number of molecules can be expressed in terms

of n_o by using the Boltzman distribution:

$$n_{TOT} = n_o + n_1 + n_2 + \ldots + n_i + \ldots$$

but:

$$n_i = n_o \frac{g_i}{g_o} \exp\left(-\Delta E_i/KT\right)$$

$$n_{TOT} = n_o + \frac{n_o g_i}{g_o} \exp\left(-\Delta E_i/KT\right) + \ldots + \frac{n_o g_i}{g_o} \exp\left(-\Delta E_i/KT\right)$$

$$+ \ldots + \frac{n_o g_N}{g_o} \exp\left(\Delta E_N/KT\right)$$

where the Nth level is the one of highest energy.

One can simplify the above equation to the form:

$$N_{TOT} = \frac{n_o Z}{g_o} \tag{56}$$

where Z is known as the partition function:

$$Z = \sum_{i=o}^{N} g_i \exp\left(-\Delta E_i/KT\right)$$

Returning to equations (46) and (48), we have:

$$N_{TOT} = n_i \frac{g_o}{g_i} \exp\left(-\Delta E_i/KT\right) \frac{Z}{g_o}$$

which yields:

$$\frac{n_i}{N_{TOT}} = \frac{g_i \exp\left(-\Delta E_i/KT\right)}{Z} \tag{57}$$

The ratio of the number of molecules in the J'th rotational level relative to the total number of molecules in the ν=0 state is obtained using equations (55) and (57)

$$\frac{N_{J'}}{N_{TOT}}_{\nu=0} = \frac{\exp\left(-J'(J'+1)BhC/KT\right)\ (2J'+1)}{Z_R} \tag{58}$$

where:

$$Z_R = \sum_{J=0}^{N} (2J+1) \exp(-J(J+1)Bch/KT) \qquad (59)$$

Using the same reasoning for vibrational transitions, we have initially:

$$\Delta E_\nu = hc\nu\bar{\omega}e \qquad (60)$$

where:

ν = vibrational quantum number

$\bar{\omega}_e$ = vibrational constant† = 2.990.9463 cm^{-1} (for HCl)

In the same form as equation (57), we have for vibration:

$$\frac{n_{\nu'}}{n_{TOT}} = \frac{\exp(-hc_\nu \bar{\omega}_e/KT)}{Z_\nu} \qquad (61)$$

Here n_{TOT} represents the total number of molecules in all vibrational levels.

The vibrational partition function is given by:

$$Z_\nu = \sum_{\nu=0}^{N} \exp(-hc\nu \bar{\omega}_e/KT) \qquad (62)$$

Vibrational levels are not degenerate; therefore the g_i terms do not appear. It is clear that by multiplying equations (58) and (61) together, the ratio of the number of molecules in the (ν',J') state to the total number of HCl molecules is given by:

$$\frac{n_{\nu',J'}}{n_{TOT}} = \frac{(2J'+1) \exp(-J'(J'+1)Bhc/KT) \exp(-hc_\nu'\bar{\omega}_e/KT)}{Z_R Z_\nu} \qquad (63)$$

---

†$\bar{\omega}_e$ is known as the hypothetical equilibrium frequency of the anharmonic oscillator. It is the frequency for infinitely small vibrations about the equilibrium point of the molecule.

The evaluation of the partition functions Z_R and Z_ν can at times become very tedious unless some approximations are made. This can be done for the vibrational case but not for rotation. For vibration at 1500°K, it can be shown that most of the molecules are in the $\nu=0$ state. Using the Boltzman distribution and equation (54) we have:

$$\frac{n_{\nu=1}}{n_{\nu=0}} = \exp\left(\frac{-hc\bar{\omega}_e}{KT}\right) = .056684$$

and

$$\frac{n_{\nu=2}}{n_{\nu=0}} \exp\left(\frac{-2hc\bar{\omega}_e}{KT}\right) = .0032$$

From these ratios, it is clear that:

$$n_{\nu=0} + n_{\nu=1} \simeq n_{TOT}$$

Using equation (53), we have

$$\frac{n_{\nu=0}}{n_{TOT}} \simeq \exp\frac{(-(0)hc\bar{\omega}_e/KT)}{\sum_{\nu=0}^{1} \exp(-hc\nu\bar{\omega}_e/KT)}$$

$$\frac{n_{\nu=0}}{n_{TOT}} \simeq \frac{1}{1+.056684} = .946$$

In the case of rotation at 1500°K, many levels are substantially populated and no convenient approximation can be made. Evaluation of the first 25 terms of the partition function was considered sufficient accuracy for this study because higher energy levels are thinly populated and contribute a negligible amount to the summation.

It is found that for HCl:

$$Z_R \simeq \sum_{J=0}^{25} (\quad) \simeq 60.576$$

and:

$$\frac{n_{J=7}}{n_{TOT}}_{\nu=0} = \frac{(2(7)+1)\ \exp\ (-2(7+1)BhC/KT)}{60.576} = .141$$

Finally, the ratio of $n_{\nu=0,J=7}$ to n_{TOT} is given as:

$$\frac{n_{\nu=0,J=7}}{n_{TOT}} = (.946)\ (.141) = .133$$

or:

$$n_{\nu=0,J=7} = n' = .133\ n_{TOT}$$

Effective Cross Section

The absorption cross-section is the next item that must be calculated. Unfortunately, the Einstein coefficients were not available for HCl to allow a quick calculation of the effective cross-section. However, data on dipole transition matrix elements for the fundamental and first and second overtone transitions were given for HCl and these could be used to calculate an A' coefficient and then, finally, an absorption cross-section. The frequency of a spontaneous transition from an upper level (ν',J') to a lower level (ν'',J'') is given by the expression: (ref 14:121).

$$A^{\nu',J'}_{\nu'',J''} = \frac{64\pi^4 \bar{\omega}_o^3}{3h(2J'+1)} |m| |R^{\nu'}_{\nu''}|^2 \left[\frac{1-8BM_o m}{\bar{\omega}_e M_1 r_e}\right] \qquad (64)$$

where:

$\bar{\omega}_o$ = band origin in cm^{-1}

h = Planck's constant (erg-sec)

m = -J'' (P-branch transitions)

or:

m = J''+1 (R-branch transitions)

$\left|R^{\nu'}_{\nu''}\right|$ = rotationless dipole moment transition matrix element (esu-cm)

M_0, M_1 = Dipole Moment coefficients

r_e = equilibrium distance between atoms of the molecule

The last factor in equation (64) is sometimes known as the Herman-Wallis correction factor for rotation.

Before evaluating A', the dipole transition matrix element had to be calculated. The dipole transition matrix element is defined as:

$$R^{\nu'}_{\nu''} = \int_0^\infty \psi^*_{\nu'',J''}(r) \quad M(r) \; \psi_{\nu',J'}(r) \; dr \qquad (65)$$

Numerical solution of the Schrodinger wave equation using a quintic anharmonic oscillator potential and third order perturbation theory was used (ref 15) to obtain expressions for the wavefunctions $\psi_{\nu,J}$.

A cubic dipole moment function of the form:

$$M(r)=M_0+M_1(r-r_e)+M_2(r-r_e)^2+M_3(r-r_e)^3$$

was used. The evaluation of the integral in equation (65) gives finally for the second overtone rotationless transition matrix element:

$$R^3_0 = \frac{(3)^{\frac{1}{2}}}{8} \gamma^{3/2}(M_1 r_e(a_2+\frac{3}{4}a_1^2) + 4M_2 r_e^2 a_1 + 4M_3 r_e^3)$$

where:

Dunham Potential Constants

$a_1 = -2.364$

$a_2 = 3.662$

$a_3 = -4.710$

$\gamma = \frac{B}{\omega_e} = .00708$

Dipole Moment Coefficients

$M_1 = .914$ Debye/$\mathring{A}$

$M_2 = .025$ Debye/$\mathring{A}^2$

$M_3 = -1.54$ Debye/$\mathring{A}^3$

(1 Debye = 10^{-18} esu-cm

This yields:

$$R_0^3 = -2.1559 \times 10^{-21} \text{ esu-cm}$$

Using Equation (64), the Einstein coefficient becomes:

$$A'(\nu'=3, J'=8 \rightarrow \nu''=0, J''=7) = .31396 \text{ sec}^{-1}$$

The effective absorption cross-section is given again by equations (26), (27), and (28). The line shape profiles $\sigma(\nu)$ and $L(\nu)$ are assumed to be reasonably well represented by a Doppler-broadened profile. The width of the HCl absorption line is given by equation (19) with:

$$M = (35\text{AMU})\ (1.66\text{X}10^{-27})\text{kg/AMU} = 5.81\text{X}10^{-26}\text{kg}$$

$$T = 1500^{\circ}\text{K}$$

$$\nu_o = C/\lambda = C/1.1838\ \mu\text{m} = 2.5325\text{X}10^{14}\text{HZ}$$

we have:

$$\Delta\nu_{HCl} = 1.1873\text{X}10^{9}\text{HZ}.$$

A typical dye laser linewidth of one angstrom is again assumed, or $\Delta\nu_L = 21.393\text{X}10^{9}$HZ. We can reasonably say that $\Delta\nu_L^2 >> \Delta\nu_{HCl}^2$ and make the same approximation for σ_{eff} as was done in the sodium case by using equation (30).

This yields:

$$\sigma_{eff} = 8.7093\text{X}10^{-21}\ \text{cm}^2 = 8.7\text{X}10^{-25}M^2$$

Note that this cross-section is a factor of about ten million smaller than that of sodium.

The lifetime of the fluorescence transition ($\nu'=3, J'=8 \rightarrow \nu''=0, J''=9$), which is the P(9) line of the second overtone is given by equation (64) with m=-9:

$$A'_{Fluor.} = .55637 \text{ sec}^{-1}$$

This means that the lifetime of the state is:

$$\tau = \frac{1}{A'} = 1.797 \text{ sec}$$

This is a very long lifetime, so equation (14) should be used to determine the total number of signal photons collected in a sounding period (τ_d).

Using the parameters:

I = 1 joule/pulse = 5.9617×10^{18} photons @ 1.1838 μm

Δt = 6.6 sec

N = 10 pulses

A' = .55637 sec^{-1}

σ = 8.7093×10^{-25} M^{+2}

Z = 300 KM

A = .785 M^2

η = .1

ε = .765

Θ_F = .05

Δ_Z = 10 m

$T_R = T_t$ = 1 (assuming rocket at altitudes above 70 KM)

we have:

$$N_{TOT}_{Det.} = (1.3766 \times 10^{-20}) \left(\frac{n_R}{n_T}\right) K (1-e^{-A^*\Delta t}) \sum_{i=0}^{9} \sum_{J=0}^{i} \exp(-JA^*/10)$$

The quantities (n_R/n_T) and Λ^* can be evaluated by first determining the mean time between collisions (τ_c) by using equations (16) and (17). From a rocket plume computer model run by the foreign technology division (FTD), the total number of colliding molecules (n_c) is about (5.88) times larger than the total number of HCl molecules ($\simeq 10^{17} cm^{-3}$). The average velocity of the HCl molecules is given by equation (16) with:

$m = 5.81 \times 10^{-26} kg$

$T = 1500^{o}K$

This yields a velocity of 1.034×10^{5} cm/sec.

The approach now is to choose a column density (K) and solve for $N_{\substack{TOT \\ Det.}}$

This is simplier than choosing a $N_{\substack{TOT \\ Det}}$ and arriving at a column density since much more algebra is involved. When a value for column density is specified, a value for HCl particle density (n) and total collision particle density (n_c) is also specified by the following relationships:

$$K = n'\Delta Z = (.133)\, n\Delta Z$$

and

$$n_c = 5.88n$$

If the plume is modeled to be 10 meters thick, then $\Delta Z \simeq 10$ meters. With the above values, a table of column density vs. $N_{\substack{TOT \\ Det}}$ is constructed.

Table X

Column Density vs. N_{TOT}^{Det}

K (m-2)	n (cm^{-3})	N_{TOT}^{Det} (counts)
1.33×10^{16}	10^{10}	1.00×10^{-11}
1.33×10^{20}	10^{14}	5.54×10^{-5}
1.33×10^{23}	10^{17}	1.68×10^{-5}
1.33×10^{25}	10^{19}	1.68×10^{-5}

From the results in Table X, it is clear that detection of HCl in the scenario envisioned is impossible for reasonable column densities. The main reason for the problem is the small Einstein transition coefficient and the resultant small absorption cross-section and long radiative lifetime. Small column densities result in less quenching but the slow radiative lifetime of the state results in a small number of radiative transitions occuring in the total sounding time period (τ_d). Large column densities do not help the signal because collisional deexcitation deexcites the molecule before it has a chance to radiate. This result manifests itself in the small value of the ratio (n_R/n_T) in the modified LIDAR equation. One could hope to obtain more signal counts by continuously sampling the return. In other words $\Delta t \rightarrow f_p^{-1}$. Of course in this case, one loses spatial resolution capability (ΔZ) and one is also allowing much more noise into the system. This approach could only be done in a scenario almost totally free of background noise. However this still would not help as the signal counts would never exceed 10^{-4} in the one second sounding period which can be verified by substituting (.01) in for Δt and solving the modified LIDAR equation with the same parameters as before.

Consequences of a Laser With a Broader Tunable Range

If a tunable laser were developed that could reach into the ultraviolet, then it would be possible to take advantage of the laser absorption cross-sections for electronic transitions and detection of HCl through resonance fluorescence would probably be feasible. If a tunable laser is developed that could look farther into the IR, one could take advantage of the larger absorption cross-sections and shorter radiative lifetimes of the fundamental band of HCl. If one excited the 1-0 band, the absorption cross-section would be increased by a factor by:

$$\frac{\sigma_{10}}{\sigma_{30}} = \frac{A_{10}\lambda^2_{10}}{A_{30}\lambda^2_{30}} = \frac{|R^1_o|^2 \omega^3_{10} \lambda^2}{|R^3_o|^2 \omega^3_{30} \lambda^2_{30}} = 378$$

where:

$A_{10} \simeq 48.3\ A_{30} \simeq 19\ sec^{-1}$

$\omega_{10} \simeq 3030\ cm^{-1}$

$\lambda_{10} \simeq 3.3\ \mu m$

Also, for a laser output of 1 joule, one would obtain a factor of 2.8 more photons at 3.3 μm than at 1.18 μm. Also, the quantum efficiency (θ_F) would increase by an order of magnitude since a $\nu'=1$ level can only decay to the $\nu''=0$ level. Substituting these values into the modified LIDAR equation with the parameters used above gives about 60 signal counts for ten sample times 6.6 μsec in duration. This is indeed a good signal and makes detection of HCl feasible if a laser can be found to excite the (1-0) band.

Conclusions

Detection of HCl through LIDAR fluorescence techniques appears

unlikely unless lasers of reasonable output energies can be built to excite electronic transitions in the UV or IR - vibrational-rotational lines in the fundamental band. Present dye lasers can only excite overtone bands of HCl and these have absorptions cross-sections too small for a reasonable LIDAR return.

C. Hydrogen Flouride (HF)

Choice of Transition

Another molecule which may appear in a rocket plume is HF. The first task again is to choose a transition for excitation and fluorescence. Unfortunately, like HCl, all electronic transitions in HF are in the far-ultraviolet and not accessible to the dye laser. One is forced again into excitation of vibrational-rotational transitions and must live with the resultant smaller absorption cross-sections. Given a temperture of 1500°K, equation (53) can be used to determine the most populated rotational level. In the case of HF, B = 20 cm^{-1} (ref 12:45) and substituting this into equation (53) yields:

$$J_{MAX} = 5$$

The number density of $n_{J=5}$ relative to n_{TOT} can be found by utilizing equation (58). This gives

$$n_{J=5} = (.118)\, n_{\substack{TOT \\ \nu=0}}$$

The ratio of $n_{\nu=1}$ to $n_{\nu=0}$ is given by:

$$\frac{n_{\nu=1}}{n_{\nu=0}} \simeq \exp\left(\frac{-hC\bar{\omega}e}{KT}\right)$$

using $\bar{\omega}_e = 4138.5\ cm^{-1}$ for HCl we have:

$$\frac{n_{\nu=1}}{n_{\nu=0}} = .019$$

It is clear therefore that $n_{\nu=0} \simeq (.98)\, n_{TOT}$ and the ground state of interest is therefore $\nu''=0$, $J''=5$. The ratio of ground state molecules to the total number of molecules is then, by equation (63), equal to:

$$\frac{n_{\nu''=0,J''=5}}{n_{TOT}} = \frac{n'}{n_{TOT}} = (.118)\ (.98) = (.116)$$

A transition is needed such that the exciting wavelength will be within the capability of the dye laser. Excitation from the $\nu''=0$ to $\nu'=1$ or 2 is too far out in the IR for the laser. Again, as in the case of HCl, the second overtone vibrational band must be considered if one uses a dye laser. Recalling the selection rule: $\Delta J=\pm 1$, the excitation transition is chosen to be ($\nu''=0,J''=5 \rightarrow \nu'=3,J'=6$). This is the R(5) transition.

Spectral line data on the second overtone band was not available, however, spectral lines could be calculated by using the Dunham coefficients. For the laser line we have (ref 12:74):

$$\frac{\Delta E}{hc} = \Delta\varepsilon = \frac{1}{\lambda}\ cm^{-1} = (2B(J''+1)-4D\ (J''+1)^3 + 3\bar{\omega}_e\ (1-4\chi_e))$$

where:

χ_e = vibration correction factor for the anharmonic oscillator

$$\frac{1}{\lambda} = (2(20)(6)-(4)(.00187)(6)^3+3(4138.5)(1-4(.0218)))cm^{-1}$$

$$\frac{1}{\lambda} = 11571.253\ cm^{-1}$$

Finally:

$$\lambda laser = 8642.1\ \text{Å}$$

From (ref 14:128), the ($\nu'=3 \rightarrow \nu''=2$ or ($\nu'=3 \rightarrow \nu''=1$) fluorescence are much more likely to occur than the second overtone transition since these transitions have much higher Einstein A' coefficients. Unfortunately, the $\nu'=3 \rightarrow \nu''=2$ band which has the highest A' coefficient of the three is not a desirable wavelength regime to

monitor because, like the fundamental band, it lies in the middle of the 2.7 μm water emission band which could introduce unacceptable absorption and noise into the LIDAR experiment. Thus, the $\nu'=3$, $\nu''=1$ transition is chosen.

Utilizing the selection rule $\Delta J = \pm 1$ one may observe either the ($\nu'=3, J'=6 \rightarrow \nu''=1, J''=7$) or the ($\nu'=3, J'=6 \rightarrow \nu''=1, J''=5$) which are the P(7) and R(5) transitions respectively. The P(7) transition is arbitrarily chosen. The wavelength of this transition is given by:

$$\lambda(\text{cm}) = (\Delta\epsilon_\nu - \Delta\epsilon_J)^{-1} \qquad (66)$$

where:

$\Delta\epsilon_\nu$ = Energy difference between the vibrational levels.

$$\Delta\epsilon_\nu = (\nu' + \tfrac{1}{2})\bar{\omega}_e - \chi_e(\nu' + \tfrac{1}{2})^2\bar{\omega}_e - (\nu'' + \tfrac{1}{2})\bar{\omega}_e + \chi_e(\nu'' + \tfrac{1}{2})^2\bar{\omega}_e$$

$$\Delta\epsilon_{\nu'=3,\ \nu''=1} = ((3.5)\ (4138.5) - (.0218)\ (3.5)^2\ (4138.5 - (1.5)\ (4138.5) + (.0218)\ (1.5)^2\ (4138.5))$$

$$\Delta\epsilon_{\nu'=3,\ \nu''=1} = 7374.807\ \text{cm}^{-1}$$

Calculating the rotational energy gaps and making use of the fact that the rotational correction constant is:

$$D = 4B^3/\bar{\omega}_e^2$$

we have:

$$\Delta\varepsilon_J = (BJ''(J''+1)-DJ''^2(J''+1)^2-BJ'(J'+1)+DJ'^2(J'+1)^2)$$

$$\Delta\varepsilon_{J'=6,J''=7}=((20)(56)=(.00187)(49)(64)-(20)(42)+(.00187(36)(49))$$

$$\Delta\varepsilon_J = 277.43436 \text{ cm}^{-1}$$

Returning to equation (66) we have for the fluorescence wavelength:

$$\lambda_F(\text{cm}) = 1.409\text{X}10^{-4} \text{ cm} = 1.4090 \ \mu\text{m}$$

This transition is in the IR and an InSb IR detector is better to use than a photomultiplier tube since the quantum efficiency at the fluorescence wavelength is approximately (.27).

Absorption Cross-Section

The rotationless Einstein A' coefficient for the laser wavelength was obtained from (ref 14:128). The coefficient does not include the Herman-Wallis correction factor for rotation, however this correction is usually very small and can be neglected. The value is 1.223 sec^{-1}. Using equation (28) to calculate $\Delta\nu_{HF}$ at T = 1500°K gives:

$$\Delta\nu_{HF} = 2.1516\text{X}10^9\text{HZ}$$

With a laser linewidth of $\Delta\lambda$=100pm or $\Delta\nu_L$ = .40141X10^9HZ it is clear that $\Delta\nu_L$ and $\Delta\nu_{HF}$ are close to being equal. Therefore, the complete expression for the effective cross-section, equation (21), should be used. This yields:

$$\sigma_{eff} = 1.0139 \text{ X } 10^{-22} \text{ M}^2$$

The Einstein A' coefficient for the 3-1 vibrational transition is equal to 65.44 sec^{-1} (ref 14:128).

One can now utilize equation (14) to determine K vs. $N_{\substack{TOT \\ Det}}$. Choosing the following parameters:

$I = 4.3521X10^{18} \frac{\text{photons}}{\text{pulse}}$ @ 8642.1Å

$\sigma_{eff} = 1.0139X10^{-22} m^2$

$A'_{31} = 65.44\ sec^{-1}$

$\Delta t = 6.6\ \mu sec$

$A = .785\ m^2$

$Z = 3X10^5 m$

$\eta = .27$

$\epsilon = .765$

$n' = .118n$

$N = 10$ pulses

$\sigma_c = 10^{-15}\ cm^2$

$\Delta Z = 10m$

$n_c = 2\dot{n}$ (from FTD plume model)

in equation (14), with Θ_F determined by:

$$\Theta_F = \frac{1}{2} \frac{A'_{31}}{A'_{31}+A'_{30}+A'_{32}} = .069\dagger$$

we obtain:

$$N_{\substack{TOT \\ Det}} = (1.3095X10^{-17}) \left(\frac{n_R}{n_T}\right) K \left(1-e^{-A^*\Delta t}\right) \sum_{i=0}^{9} \sum_{J=0}^{i} \exp\left(-JA^*/10\right)$$

Again, as in the case of HCl, one assumes a column density (K) and solves for $N_{\substack{TOT \\ Det}}$ which is the number of signal photons or counts registered.

---

†The factor of ($\frac{1}{2}$) in the expression for Θ_F arises because of the two equally probable rotational transitions that can occur for each vibrational transision.

Table XI

HF Column density (K) vs. Signal Counts (N_{TOT}^{Det})

K (m^{-2})	n (cm^{-3})	N_{TOT}^{Det} (counts)
1.18×10^{16}	10^{10}	6.68×10^{-4}
1.18×10^{18}	10^{12}	5.36×10^{-2}
1.18×10^{20}	10^{14}	6.10
1.18×10^{22}	10^{16}	36.90
8.73×10^{23}	7.4×10^{17}	36.90

The HF number density of 7.4×10^{17} cm^{-3} that appears in Table XI comes from the FTD rocket plume model mentioned briefly in the HCl section. From the above table, it is clear that for reasonable HF number densities (10^{17} cm^{-3}), LIDAR detection of HF seems feasible. The next question is: Is background noise at the fluorescence wavelength low enough to achieve a signal to noise greater than one?

HF Noise Analysis

From the ESA report (ref 4:42) the radiance values for terrestially reflected sunlight and moonlight at the fluorescence wavelength (1.4 μm) are given as:

$$L_E = 1.3636 \times 10^{17} \frac{\text{photons}}{m^2 \text{ str. sec } \mathring{A}}$$

and:

$$L_M = 2.4242 \times 10^{11} \frac{\text{photons}}{m^2 \text{ str. sec } \mathring{A}}$$

Using equation (40) with:

$\theta_D = 3.33 \times 10^{-5}$ rad (yields a spot size of 10 meters at 300km)

$\Delta\lambda = 1\text{Å}$

we can determine the number of background photons detected to be:

$$N_E = 127.3 \text{ photons detected/sample time}$$

$$N_M = 2.32 \times 10^{-5} \text{ photons detected/sample time}$$

Using these values in equation (41) without the factors of δ since a photomultiplier tube cannot be used here at 1.4 μm, we can determine the minimum number of signal counts (N_{min}) per sample time to obtain a certain signal to noise (R). For daylight observations, N_E dominates all noise terms and at night we have only N_M. N_d is again considered to be negligible. With the above values, tables of N_{min} vs. R are given for day and night soundings.

Table XII

Day N_{min} vs. R at 1.4 μm

N_{min} (Counts/sample time)	R Signal/Noise)
3.62	1
7.34	2
11.16	3
15.09	4

Table XIII

Night N_{min} vs. R at 1.4 μm

N_{min} (Counts/sample time)	R (Signal/Noise)
.100	1
2.5	5
10.0	10
40.0	20

The above tables show that daylight soundings of HF are just feasible given the scenario used in this thesis since a signal count of at least 36.2 is needed in ten sample times. The best that can be done from Table XI is about 36.9 counts. Nighttime soundings look much more promising. A signal count of 36 will yield a signal to noise of about six.

Beam Divergence

A beam divergence of 3.33×10^{-5} radians was used in this analysis so that the laser spot size would be on the order of the plume size (about 10 meters). To determine if the laser needs expanding optics or not, it is necessary to make an estimate of the exit aperature required at the laser to obtain the above Θ_D. Using equations (43) and (44), an exit aperature of 4.32 cm is required. With this size beam, expanding optics are probably necessary.

Conclusions

Detection of HF through LIDAR techniques does appear to be feasible if the soundings are done at night. As in the case of HCl, if tunable lasers are developed that can operate in the UV or IR beyond 3 μm, then

HF detection should be much easier. Sounding periods longer than 1 second should also contribute more signal counts to the LIDAR receiver and it is quite likely that extended soundings could be carried out in daylight with acceptable signal to noise. Extended soundings were not considered, as mentioned previously, to avoid a complicated integration over aspect angle (Θ) with time.

D. Diatomic Iodine (I_2)

Diatomic iodine is a molecule of interest because various isotopes of molecular iodine are by-products of nuclear explosions. Thus, detection of I_2 in a localized area of the atmosphere through LIDAR techniques could be a promising way of remotely monitoring nuclear testing activity around the world. Ideally, iodine molecules involving isotopes I^{131}, I^{133}, or I^{135} should be considered in the LIDAR analysis, however, only sufficient data on I_2^{127} was available, so this molecule was analysed. It is believed that the diatomic iodine with various isotopes should have comparable absorption cross-sections, but the wavelengths of the various transitions will vary from isotope to isotope. The basic scenario considered is the space shuttle LIDAR platform in a 250KM circular orbit and the I_2 cloud lying in the range of 30,000 to 50,000 ft. (9-15KM). Look angles of 0^o (nadir), 30^o and 45^o are considered. A 1 joule per pulse, 10 PPS dye laser is again considered and a total sounding time of one second is assumed to allow Θ to remain constant. A sample time (Δt) of 6.6 μsec is used. The cloud is considered relatively hot at 500^oK, consistant with the expected conditions shortly after a nuclear blast. The receiver aparature is .785 M^2 (1 meter in diameter).

Transition

Fortunately, the first few electronic transitions of I_2 are in the visible wavelengths and are thus accessible to the dye laser. The electronic transition $X'\Sigma \rightarrow B^3\pi$ is chosen. The Franck-Condon principal favors the vibrational transition $\nu''=0 \rightarrow \nu'=25$ (ref 17). The rotational fine structure transition of interest will be determined by what J"

level is the most populated at 500°K. Using equation (53) with $B = .03729\ cm^{-1}$ (ref 18), we find that $J''_{max} = 68$. Therefore, we may excite either ($X'\Sigma, v''=0$, $J''=68 \rightarrow B^3\pi, v'=25, J'=69$ or 67) lines which are respectively, the R(68) or P(68) lines. The fluorescence emission lines of interest are:

$$B^3\pi, v'=25 \rightarrow X'\Sigma, v''=0$$

and:

1) $J'=69 \rightarrow J''=68$ R(68)

2) $J'=69 \rightarrow J''=70$ P(70)

3) $J'=67 \rightarrow J''=66$ R(66)

4) $J'=67 \rightarrow J''=68$ P(68)

The R(68) line is chosen arbitrarily for laser excitation. This leaves a choice of (1) or (2) above for the fluorescence wavelength. The P(70) transition is chosen for fluorescence since a wavelength other than the laser wavelength is desired for detection to eliminate background from Mie scattering. The laser and fluorescence wavelengths are given respectively as:

$$\lambda_{laser}(cm) = \left(\Delta\epsilon_{X'\Sigma \rightarrow B^3\pi} + \Delta\epsilon_{v''=0 \rightarrow v'=25} + \Delta\epsilon_{J''68 \rightarrow J'=69}\right)^{-1}$$

and:

$$\lambda_F(cm) = \left(\Delta\epsilon_{B^3\pi \rightarrow X'\Sigma} + \Delta\epsilon_{v'=25 \rightarrow v''=0} + \Delta\epsilon_{J'=69 \rightarrow J''=70}\right)^{-1}$$

where:

$$\Delta\epsilon_{X'\Sigma \rightarrow B^3\pi} = \Delta\epsilon_{B^3\pi \rightarrow X'\Sigma} = 15769.01\ cm^{-1}\ \text{(ref 16)}$$

and:

$$\Delta\epsilon_{v''=0 \rightarrow v'=25} = \Delta\epsilon_{v'=25 \rightarrow v''=0} = \left|\epsilon_{v'=25} - \epsilon_{v''=0}\right|$$

where:

$$\varepsilon_\nu = \omega_e(\nu + \tfrac{1}{2}) - \omega_e\chi_e(\nu + \tfrac{1}{2})^2 + \omega_e Y_e\ (\nu + \tfrac{1}{2})^3 + \omega_e Z_e(\nu + \tfrac{1}{2})^4$$

The vibrational coefficients change depending on what electronic level the molecule is in, therefore:

$$\Delta\varepsilon_{vib} = \omega_e'\ (25 + \tfrac{1}{2}) - \omega_e'\chi_e\ (25 + \tfrac{1}{2})^2 + \omega_e'Y_e'\ (25 + \tfrac{1}{2})^3$$

$$+\omega_e'Z_e'\ (25 + \tfrac{1}{2})^4 - \omega_e''\ (\tfrac{1}{2}) + \omega_e''\chi_e''\ (\tfrac{1}{2})^2$$

$$-\omega_e''Y_e''\ (\tfrac{1}{2})^3 - \omega_e''Z_e''\ (\tfrac{1}{2})^4$$

Using the vibrational constants from (ref 17:25) and (ref 18:40); we obtain:

$\omega_e' = 125.273\ cm^{-1}$

$\omega_e'\chi_e' = .7016\ cm^{-1}$

$\omega_e'Y_e' = .00567\ cm^{-1}$

$\omega_e'Z_e' = 3.2x10^{-5}\ cm^{-1}$

$\omega_e'' = 214.5\ cm^{-1}$

$\omega_e''\chi_e'' = .60738\ cm^{-1}$

The higher order double primed vibrational terms contribute little to $\Delta\varepsilon_\nu$ and are ignored. Substituting these vibrational constants into the above equation, we obtain:

$$\Delta\varepsilon_\nu = 2550.6619\ cm^{-1}$$

The rotational energy is computed using the formula:

$$\Delta\varepsilon_{J'',J'} = ((B' + B'')\ (J'' + 1) + (B'-B'')\ (J'' + 1)^2) \qquad (67)$$

where B' and B" represent respectively the rotational constant values for the upper and lower electronic states. The B coefficients were determined from the formula:

$$B = B_e - \alpha_e (\nu + \tfrac{1}{2}) + \gamma_e (\nu + \tfrac{1}{2})^2 + \delta_e (\nu + \tfrac{1}{2})^2 \qquad (68)$$

where the coefficients are correction factors to the rotational constants due to changes in the equilibrium distance between the two iodine atoms due to variations in vibrational energy. These correction factors, like the vibration case, can change depending on what electronic state the molecule is in. For the ground electronic state we have (ref 18:40):

$$B_e'' = .037389 \text{ cm}^{-1}$$

$$\alpha_e'' = .000121 \text{ cm}^{-1}$$

The other terms are neglegible for $\nu''=0$.

The rotational coefficients for the upper elctronic state are (ref 17:25):

$$B_e' = .028969 \text{ cm}^{-1}$$

$$\alpha_e' = .0001562 \text{ cm}^{-1}$$

$$\gamma_e' = 4X10^{-7} \text{ cm}^{-1}$$

$$\delta_e' = 3.5X10^{-8} \text{ cm}^{-1}$$

By substituting these values into equations (67) and (68), we obtain:

$$\Delta\varepsilon_{J''=69 \rightarrow J'=69} = 20.046053 \text{ cm}^{-1} \text{ for the laser}$$

and

$$\Delta\varepsilon_{J''=69 \rightarrow J'=70} = 30.423376 \text{ cm}^{-1} \text{ for the fluorescence.}$$

Finally:

$$\lambda_{laser} = (15769.01 + 2550.6619 - 20.046053)^{-1} \text{ cm}$$

$$\lambda_{fluor.} = (15769.01 + 2550.6619 - 30.423376)^{-1} \text{ cm}$$

which gives 5464.1Å and 5467.2Å for the laser and fluorescence wavelengths respectively. Since the laser and fluorescence wavelengths are very close to each other, a narrower laser linewidth than that used previously is chosen so that there is no chance of the laser beam exciting other hyperfine rotational lines.

Fluorescence Efficiency

The fluorescence efficiency (Θ_F) is the product of the Franck-Condon factor and the rotational factor. From (ref 19:329) the Franck-Condon factor for the $\nu'=25 \rightarrow \nu''=0$ transition is given as (.027). The J =69 rotational state can decay into two different lower state rotational levels J" =70 and J" =68 with equal probability. Therefore the fraction of the total number of molecules in the $\nu'=25$, J'=69 state that will decay to the $\nu''=0$, J"=70 level is:

$$\Theta_F = (.5)\ (.027) = .0135$$

Absorption Cross-Section

The linewidth of the Doppler-broadened profile is given by equation (24) with:

$\nu_o = 5.4867X10^{14}$ HZ

$T = 500^oK$

$M = 2(127\ AMU)\ (1.66X10^{-24} g/AMU) = 4.2164X10^{-22}$ g

Using equation (27) we have:

$\Delta\nu_{I_2} = 5.4965X10^8 HZ$

and

$$\Delta\nu_L = \frac{C\Delta\lambda_L}{\lambda^2} = \frac{2.998X10^8 \frac{m}{sec}(.1\text{Å})}{(5464.1\ \text{Å})^2} = 110.46X10^8\ HZ$$

Again we have $\Delta\nu_L >> \Delta\nu_{I_2}$, and we may use the approximation for the effective cross-section, equation (30). From (ref 20:1381) the lifetime (τ) of the ($B^3\pi \rightarrow X^1\Sigma; \nu'=25 \rightarrow \nu''=0$) transion is given as $7.2X10^{-7}$ sec. The rotational fine structure within the vibronic transitions do not significantly perturb the A' value, and so these small corrections are ignored. Using equation (26) with:

$$\frac{g_b}{g_a} = \frac{2J'+1}{2J''+1} = \frac{2(69)+1}{2(70)+1} = .9858$$

and

$$\lambda = 5467.2 \text{ Å}$$

we have:

$$\sigma_{eff} = 1.5252X10^{-14} \text{ cm}^2 = 1.5252X10^{-18} \text{m}^2$$

LIDAR Receiver

The 7265 RCA photomultiplier tube seems to be a good choice for detection of the fluorescence (ref 5:211). The photocathode (Na Sb K Cs) has a relatively high responsivity and a quantum efficiency at 5461 Å of about (.1). The throughput factor (ε) is the same as that used for sodium. The reflectivities of the mirrors within the detector telescope have basically the same values at 5461 Å as they had for the sodium wavelength at 5896 Å.

Transmission

A table of transmissivity vs. penetration depth (χ) into the atmosphere was generated by interpolation between transmission values for the 5461 Å and 6328 Å laser lines in the same manner as explained in the sodium section. Finally, a table of transmission vs. penetration depth into the atmosphere was generated (Table XIV). As in the case

of sodium, penetration depth (χ) is defined as zero kilometers at 100 KM above the earth and 100 KM at ground level.

Table XIV

Transmission vs. Penetration Depth at 5462 Å

χ	τ	χ	τ	χ	τ
30	.9992	80	.9896	91	.9352
50	.9990	81	.9868	92	.9275
55	.9989	82	.9834	93	.9193
60	.9987	83	.9796	94	.9106
65	.9983	84	.9755	95	.9007
70	.9973	85	.9711	96	.8864
75	.9967	86	.9662	97	.8590
76	.9958	87	.9609	98	.7991
77	.9947	88	.9551	99	.6654
78	.9934	89	.9489	100	.4096
79	.9917	90	.9423		

It is assumed that the natural concentration of I_2 in the atmosphere is small enough so that losses due to resonance absorption (K_m) is nearly zero.

Noise Analysis

The noise analysis follows the same general procedure as outlined in the sodium case. Once again the curves in ref 4:42 were used to determine radiances of reflected sunlight and moonlight off of the earth at 5461 Å. This fluorescence wavelength does not lie on a Fraunhofer absorption line; thus noise values for I_2 will be greater than those for sodium. The radiances of reflected sunlight and moonlight at 5461 Å are respectively:

$$L_E = 1.7424 \times 10^{17} \text{ photons/sec Å str m}^2$$

and

$$L_M = 2.1818 \times 10^{12} \text{ photons/sec Å str m}^2$$

Returning to equation (40) with:

$A = .785\ m^2$

$\Theta_D = 10^{-4}$ rad

$\Delta\lambda = .5\ \overset{o}{A}$

$\eta = .1$

$\epsilon = .765$

$\Delta t = 6.6\ \mu sec$

The number of noise photons detected per sample time is:

$N_E = 278.29$ photons/sample time

$N_M = 3.48 \times 10^{-3}$ photons/sample time

The noise due to dark current can again be neglected if the photocathode is cooled to 220°K. Using equation (41), one can determine the minimum number of signal photons (N_{min}) required to give a particular signal to noise ratio (R) for daylight and night observations. Using the standard LIDAR values of laser pulse frequency (f_p) equal to 10 Hertz, LIDAR sounding time (τ_d) of 1 second and dynode gain (δ) of 3.38, Tables XV and XVI present N_{min} vs. R first for daylight observations and then nighttime.

Table XV

Iodine N_{min} vs. R

(Daylight)

N_{min}	R
6.36	1
12.86	2
26.31	4
70.37	10
157.31	20
207.70	25

Note that N_{min} (I_2) > N_{min} (Na), this is mainly due to the Fraunhofer

attenuation effect which is present for sodium but not for iodine.

Table XVI

Iodine N_{min} vs. R.

(Nighttime)

N_{min}	R
.145	1
.572	2
2.28	4
14.2	10
56.83	20
88.79	25

Note that the nighttime values are comparible to those of sodium. This is because the noise terms at night are so small that they can be neglected. The only appreciable noise is the signal noise and this is the same for both I_2 and sodium. By choosing a desired signal-to-noise value (R), one can express the minimum column density required as a function of range, look angle and laser energy per pulse by using equation (1). For R=10, equation (1) yields $N=N_{min} = 70.37$. Tables of minimum column density (K_{min}) vs. laser energy per pulse can be constructed for daylight and night soundings (Tables XVII and XVIII).

Table XVII

Daylight Minimum Detectable Column Density
vs. Laser Energy - Iodine

I (Joules/pulse)	K_{min} (10^{-16} m^{-2})
1.0	1.52
.8	1.90
.6	2.54
.4	3.81
.2	7.63
.1	15.2
.01	152.0
.002	762.0

Table XVIII

Night Minimum Detectable Column Density vs. Laser Energy - Iodine

I Joules/pulse	K_{min} (10^{16} m^{-2})
1.0	.307
.8	.385
.6	.511
.4	.770
.2	1.54
.1	3.07
.01	30.7
.002	154.0

Tables XVII and XVIII utilized the following values:

Δt = 6.6 μsec

ΔZ = 1KM

$\eta\varepsilon$ = .0765

Z = 235 KM

$\Theta = 0^{o}$

Θ_F = .0135

R = 10

Shuttle altitude = 250 KM

$\sigma = 1.52X10^{18}$ m^2

A table of minimum column density vs. range and look angle for daylight and night observations is presented next in Table XIX. The parameters not varied are the same as the ones used in Tables XVII and XVIII. The laser energy per pulse was fixed at one joule.

Table XIX

Minimum Detectable Column Density vs. Range and Look Angle - Iodine

Z_V (KM)	Z (KM)	Θ (Deg)	$(T_r T_t)^{\sec \Theta}$	K_{Day} ($10^{16} M^{-2}$)	K_{Night} ($10^{15} M^{-2}$)
150	100	0	1.0	.26	.53
175	175	0	.998	.80	1.61
200	200	0	.998	1.04	2.10
215	215	0	.996	1.21	2.44
235	235	0	.943	1.52	3.07
237	237	0	.924	1.58	3.19
240	240	0	.887	1.69	3.41
243	243	0	.846	1.81	3.66
245	245	0	.812	1.92	3.89
248	248	0	.640	2.50	5.04
150	173.21	30	1.0	.78	1.58
175	202.07	30	.998	1.06	2.14
200	230.94	30	.998	1.39	2.80
215	248.26	30	.995	1.61	3.25
235	271.35	30	.934	2.05	4.15
237	273.66	30	.913	2.13	4.30
240	277.13	30	.871	2.29	4.63
243	280.59	30	.824	2.49	5.00
245	282.90	30	.786	2.65	5.33
248	286.37	30	.597	3.57	7.22
150	212,13	45	1.0	1.17	2.36
175	247.49	45	.997	1.60	3.22
200	282.84	45	.997	2.09	4.22
215	304.06	45	.994	2.42	4.89
235	332.34	45	.920	3.12	6.30
237	335.17	45	.894	3.27	6.59
240	339.41	45	.844	3.55	7.15
243	343.65	45	.789	3.89	7.85
245	346.48	45	.745	4.19	8.44
248	350.72	45	.532	6.00	12.1

Note that it is assumed that $T_r = T_t$ which is a good approximation since the wavelengths differ by only 3 Angstroms. Finer divisions of Z between 235-248 KM were made since the I_2 cloud is considered to lie at an altitude of 9-15 Km above the earth.

Beam Divergence

A laser beam divergence of 10^{-4} radians was considered adequate for LIDAR sounding of I_2 (ref 4:31). To confirm this, one can solve equation (35) with Z equal to 350 KM which is the worse case considered here. This yields a spot size diameter of 35 meters which is probably smaller than the extent of the I_2 cloud. With θ_D equal to 10^{-4} radians, one can calculate the required exit aperature of the LIDAR transmitter using equation (36). The aperture diameter turns out to be 6.7 millimeters. Therfore, no expanding optics are necessary because the beam exiting the laser will probably be just a few millimeters wide.

Conclusions

In general, the required column densities are a thousand times greater for diamotic iodine than they are for sodium. However, they are still very small densities and detection of I_2 after a nuclear explosion seems to be promising.

E. Diatomic Hydrogen (H_2)

Diatomic hydrogen is of interest because its detection around an industrial complex may indicate possible activities involving nuclear processes. Unfortunately again, electronic transitions of H_2 are too far out in the ultraviolet to be accessible to the Dye laser. Vibration-rotation levels are the only possibilities for dye laser excitation. Diatomic hydrogen has no permanent dipole moment, and so only quadrapole transitions are allowed. The lifetimes of these transitions are on the order of 10^6 seconds (ref 22:133) which means that the effective absorption cross-section is roughly six orders of magnitude smaller than that of HCl. Since LIDAR detection of HCl is marginal at best because of it's absorption cross-section, it is clear that LIDAR detection of H_2 through vibrational-rotational excitation is impossible unless a tunable ultraviolet laser is developed to access the larger absorption cross-sections of electronic transitions.

F. Hydrogen-Tritium (HT)

HT, like H_2, is of interest because it may also indicate nuclear activity if detected in an industrial area. Unfortunately, LIDAR detection of this molecule seems unlikely because it probably has a very small permanent dipole moment. This conclusion was reached after discovering that HD (hydrogen-deuterium) has a permanent dipole moment four orders of magnitude smaller than HCl (ref 16:259). Since HT and HD differ by only one neutron, it is suspected that they have similar dipole moments. If this is true, then in all probability the dipole moment transition matrix elements ($|R^{\nu',J'}_{\nu'',J''}|$) are very small since these matrix elements depend on M(r) (see equation 57). Since the absorption

cross-section is proportional to the square of the transition matrix element, it too will be small. Therefore, it appears that detection of HT is impossible with present day technology. Electronic transitions again are too far out in the ultraviolet for today's tunable lasers.

G. Xenon (Xe) and Krypton (Kr)

Xenon and krypton are possible by-products of a nuclear blast. Therefore, they are of interest for the same reason as diatomic iodine. Unfortunately, these elements cannot be detected with a tunable dye laser because the transition from the ground state to the first excited state for both atoms is in the ultraviolet. Of course, since krypton and xenon are atoms, there is no vibrational-rotational spectra to excite. As mentioned before, a tunable dye laser that can operate in the ultraviolet is the only means of conducting LIDAR resonance scattering techniques on Xenon and krypton.

H. Boron Oxide (B_2O_3), Boric Acid (HBO_2) and Aluminum Oxide (Al_2O_3)

These molecules are interesting because their detection in a rocket plume may allow identification of the rocket fuel being used and perhaps allow determination of the vehicle performance. Very little data was found on these molecules especially in the absorption cross-section area, which, from the work of this thesis, appears to be the most important parameter to determine. Some data was gathered on the molecular spectra of gaseous HBO_2 and B_2O_3 and this data is presented in Tables XX and XXI for possible use for anyone following up on this study (ref 23:269) and (ref 24:298). No significant data on aluminum oxide was found.

Table XX

HBO_2 Spectral Data

Band	Band Center (cm^{-1})
B=O Stretch	4.97 μm
O-H Stretch	2.27 μm

Table XXI

B_2O_3 Spectral Data

Band	Spectral Location (cm^{-1}) $B_2{}^{10}O_3$	$B_2{}^{11}O_3$
ν_1(B=O Symmetric Stretch)	2087	2021
ν_2(B=O Symmetric Stretch)	760	757
ν_3(O-B-O Symmetric Bend)	498	478
ν_4(B-O-B Bend)	236	235
ν_6(B=O Asymmetric Stretch)	2095	2029
ν_7(B-O Asymmetric Stretch)	1270	1268
ν_8(O-B-O Asymmetric Bend)	568	519
ν_9(Out of Plane Bend)	493	478

I. Tritiated Water (HTO)

Like H_2 and HT, detection of tritiated water around an industrial complex may indicate nuclear activity in the area. Very little data was obtained on HTO, and so an extended analysis of this molecule was not possible. However, it may be possible to use absorption cross-sectional data of ordinary H_2O and utilize this for HTO. From (ref 6:106) absorption cross-section values in the visible (6944 Å) range of the spectrum were found to lie in the range of 10^{-23} cm^{-2}. This is not a particularly impressive cross-section and it appears that HTO sounding in the visible spectral regime will be very difficult. Spectral data was obtained (ref 25:454) and the findings are tabulated in Table XXII.

Table XXII

HTO Spectral Data

Band	Spectral Location (cm^{-1})
Bending	1324
Symmetric Stretch	2300
Asymmetric Stretch	3711
Asymmetric Stretch†	7221
Symmetric Stretch†	4565
Bending†	2643
Bending††	3933
Sym-Asym Stretch	6022
Bend†-Asym Stretch	6322
Sym Stretch-Bend†	4929
Bend-Asym Stretch	5032

† - 1st overtone

†† - 2nd overtone

V. Conclusions and Recommendations

It appears that LIDAR detection of sodium,hydrogen fluoride and diatomic iodine is very promising. This is due primarily to the large absorption cross-sections that the three species possess. The absorption cross-section was found to be the main parameter determining if a species could or could not be detected through LIDAR techniques.

Diatomic hydrogen and hydrogen tritium had very small vibrational-rotational absorption cross-sections and thus were unlikely candidates for LIDAR sounding. Hydrogen chloride had a better cross-section but was still small enough to say that its detection through resonance fluorescence techniques would be marginal at best. Xenon and krypton are, of course, not molecules; thus they had no vibration-rotation spectra. They must be excited electronically. The transition from ground state to the first excited electronic state unfortunately lies too far out in the ultraviolet and beyond the capabilities of a dye laser. They therefore cannot presently be detected through the resonance technique.

Cross-sectional data on boric acid, boron oxide and aluminum oxide could not be found, and so these molecules were not analysed in detail. Finding these cross-sections are essential if future work is to be done in this area. The development of a tunable ultraviolet laser would make detection of most of these atoms and molecules feasible because one could then access the relatively hugh electronic absorption cross-sections of the particles. Einstein (A') coefficients for hot band transitions ($\Delta v=1, v''=0$) may be useful information to obtain because some of these transitions have higher absorption cross-sections.

Refinements of work presented here would involve using computer codes such as HITRAN developed by AFGL to obtain much more precise transmission coefficients for the laser and fluorescence lines. Longer sounding scenarios should be examined to see if signal to noise can be improved significantly. This will require a small computer code to account for the changes in look angle and range.

Bibliography

1. McClatchey, R.A. et. at. Optical Properties of the Atmosphere (Third Edition). AFCRL-72-0497, 1972.

2. Mitchner, M. and Charles H. Kruger Jr. Partially Ionized Gases. New York: Wiley-Interscience, 1973.

3. McGee, T.J. and T.J. McIlrath. "Stratospheric Temperature and Pressure Determinations from an OH Fluorescence LIDAR Instrument," Applied Optics, 18(11): 1710-1714 1970.

4. Spacelab borne LIDAR for Atmospheric Research, Phase A study, Volume 1: Systems Analysis. Centre National d'Etudes Spaticles, France.

5. Shuttle Atmospheric LIDAR Research Program. NASA SP-433, 1979.

6. Hinkley, E.D. "Laser Monitoring of the Atmosphere," Topics in Applied Physics, Volume 14 Pg 206. Berlin, Heidelberg New York: Springer Verlay, 1976.

7. Pressley, R.J. Handbook of Lasers with Selected Data on Optical Properties. Cleveland, Ohio: The Chemical Rubber Co., 1971.

8. Whitten, R.C. and I.G. Poppoff. Fundamentals of Aeronomy. New York: John Wiley and Sons Inc., 1971.

9. Reich, Herbert J. Principals of Electron Tubes. New York: McGraw-Hill Books Co., Inc., 1941.

10. RCA Photomultiplier Manual. RCA Pt-61, 1970.

11. Hinkley, E.D. "Laser Monitoring of the Atmosphere" Topics in Applied Physics, Volume 14, page 257. Berlin, Heidelburg, New York: Springer Verlay, 1976.

12. Banwell,, C.N. Fundamentals of Molecular Spectroscopy. London: McGraw-Hill, 1972.

13. Ludwig, C.B. et. al. Handbook of Infrared Radiation from Combustion Gases. NASA SP-3080, 1973.

14. Sileo, R.N. and T.A. Cool. "Overtone Emission Spectroscopy of HF and DF: Vibrational Matrix Elements and Dipole Moment Function," The Journal of Chemical Physics, 65 (1): 117-133 (July 1976).

15. Toth, R.A. et. al. "Dipole Moment Matrix Elements for the 1-0, 2-0, and 3-0 Vibration-Rotation Bands of Diatomic Molecules," Journal of Molecular Spectroscopy, 23: 74-84 (1969).

16. Huber, K.P. and G. Hertzberg. Constants of Diatomic Molecules. New York: Van Nostrand Reinhold Co., 1979.

17. Steinfield, J.I., et. al. "Spectroscopic Constants and Vibrational Assignment for the $B^3\pi_{ou}^+$ State of Iodine," The Journal of Chemical Physics, 42 (1): 25-35 (1965).

18. Rank, D.H. and B.S. Rao. "Molecular Constants of the Ground State of I_2." Journal of Molecular Spectroscopy, 13: 34-42 (1964).

19. Halmann, M. et. a. "Franck-Condon Calculations for Iodine Using a Morse Potential," Journal of Molecular Spectroscopy, 21: 328-332 (1966).

20. Brewer, L., et. a. "Radiative Lifetime of I_2 Fluorescence, $B^3\pi_{o+u} \rightarrow X'\Sigma_{o+g}^{"}$ The Journal of Chemical Physics, 38 (6): 1381-1388 (1963).

21. Black, J.H. and A. Dalgarno, "Intersteller H_2: The population of excited rotational states and the Infrared Response to Ultraviolet Radiation," The Astrophysical Journal, 103: 132-142 (1976).

22. Capelle, G.A. and H.P. Broida. "Lifetimes and Quenching Cross-Sections of I_2 ($B^3\pi_{o+u}$)," The Journal of Chemical Physics, 58(10: 4212-4222 (1973).

23. Boyer, D.W. "Shock Tube Measurements of the Band Strengths of HBO_2 and OBF in the Short Wavelength Infrared," Journal of Quantitative Spectroscopic and Radiative Transfer, 24: 269-282 (1980).

24. Weltner, W. Jr. and J.R.W. Warn. "Matrix Isolation of High-Temperature Vapors: Boric Oxide," The Journal of Chemical Physics, 38(2): 292-303 (1962).

25. Carney, G.D., et. a. "Vibrational Energies for Isotopically Substituted Water: Application to Laser Isotope Separation," Applied Spectroscopy, 30(4): 453-455 (1976).

26. Bowman, M.R., et. a. "Atmospheric Sodium Measured by a Tuned Laser Radar," Nature, 221: 456-457 (1969).

Vita

Glenn Charles Kweder was born on 16 November 1951 in Pittsburgh, Pennsylvania, the son of Charles J. Kweder and his wife, Mary Fuchs. In December 1974 he received his bachelor's degree in physics and was commissioned a second Lieutenant in the United States Air Force through the ROTC program at Duquesne University in Pittsburgh, Pennsylvania. In September of 1976 he was assigned to the Air Force Weapons Laboratory where he served as the expert in the satellite laser vulnerability field. He received the Air Force Commendation award for his work at the Weapons Laboratory prior to his enrollment in the Air Force Institute of Technology in 1980.

UNCLASSIFIED

SECURITY CLASSIFICATION OF THIS PAGE *(When Data Entered)*

REPORT DOCUMENTATION PAGE		READ INSTRUCTIONS BEFORE COMPLETING FORM
1. REPORT NUMBER AFIT/GEP/PH/81D- 5	2. GOVT ACCESSION NO.	3. RECIPIENT'S CATALOG NUMBER
4. TITLE *(and Subtitle)* REMOTE SENSING OF GASES USING LIDAR RESONANCE SCATTERING TECHNIQUES FROM THE SPACE SHUTTLE		5. TYPE OF REPORT & PERIOD COVERED MS THESIS 6. PERFORMING ORG. REPORT NUMBER
7. AUTHOR(s) Glenn C. Kweder, Capt., USAF		8. CONTRACT OR GRANT NUMBER(s)
9. PERFORMING ORGANIZATION NAME AND ADDRESS AIR FORCE INSTITUTE OF TECHNOLOGY DEPARTMENT OF PHYSICS WRIGHT-PATTERSON AFB OH 45433		10. PROGRAM ELEMENT, PROJECT, TASK AREA & WORK UNIT NUMBERS
11. CONTROLLING OFFICE NAME AND ADDRESS		12. REPORT DATE Dec 1981 13. NUMBER OF PAGES 85
14. MONITORING AGENCY NAME & ADDRESS*(if different from Controlling Office)*		15. SECURITY CLASS. *(of this report)* UNCLASSIFIED 15a. DECLASSIFICATION/DOWNGRADING SCHEDULE

16. DISTRIBUTION STATEMENT *(of this Report)*

Approved for public release; distribution unlimited

17. DISTRIBUTION STATEMENT *(of the abstract entered in Block 20, if different from Report)*

18. SUPPLEMENTARY NOTES

APPROVED FOR PUBLIC RELEASE: IAW AFR 190-1.

4 JUN 1982

AIR FORCE INSTITUTE OF TECHNOLOGY (ATC)
WRIGHT-PATTERSON AFB, OH 45433

Lynn Wolaver

LYNN E. WOLAVER
Dean for Research and Professional Development

19. KEY WORDS *(Continue on reverse side if necessary and identify by block number)*

Laser
LIDAR
Remote Sensing
Space Shuttle
Resonance Scattering

20. ABSTRACT *(Continue on reverse side if necessary and identify by block number)*

Remote sensing from the space shuttle utilizing laser-induced fluorescence techniques was investigated. A feasibility study of LIDAR (Light Detection and Ranging) techniques to detect twelve gases of scientific and military interest was carried out. Evaluation of a European Space Agency LDIAR hardware design was also a task. The main emphasis was on determination of background noise, spectral transitions, atmospheric transmission and molecular absorption cross-section of the target in order to determine the minimum target concentration

Cont'd

DD FORM 1 JAN 73 1473 EDITION OF 1 NOV 65 IS OBSOLETE

UNCLASSIFIED

SECURITY CLASSIFICATION OF THIS PAGE *(When Data Entered)*

Abstract (con'td)

required to be detectable. Atomic sodium, molecular iodine and hydrogen flouride were determined to be promising candidates for LIDAR resonance detection. Other molecules investigated, such as hydrogen chloride, xenon and krypton were considered marginally detectable at best because of their small absorption cross-sections. Lack of sufficient data prevented extended analysis of the remaining molecules.

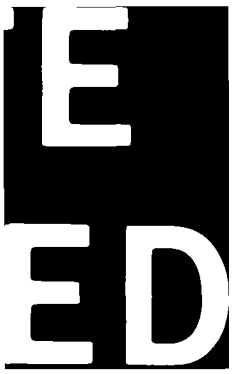
E
ED